

Scientific Highlights

Solar Energy Research 2007/2008

Breakthrough: using temperature-stable ZnO on poly-Si thin film solar cells	80
Photoconductivity in Single Si/SiO ₂ Quantum Wells	82
Room temperature electrical detection of spin coherence in C ₆₀	84
In ₂ S ₃ buffer layers for chalcopyrite solar cells	86
Beyond conventional thin films: growth and characterisation of chalcopyrite nanocrystals	88
Solar cells based on ZnO nanorod arrays with extremely thin sulphide absorber	90
Electronic properties of grain boundaries in polycrystalline, chalcopyrite-type thin films in solar cells	92
Insights into structure and microstructure of thin films by grazing incidence X-ray diffraction	94
We have take off: Cu(In,Ga)Se ₂ thin film solar cells – recent developments in space applications	96
In-situ control and verification of single-domain III-V growth on Si substrates	98
The Ultrafast Temporal and Spectral Characterisation of Electron Injection in ZnO and TiO ₂ based hybrid systems	100
Development of a membrane for photo-induced hydrogen generation	102
Preparation of photoactive WS ₂ nanosheets by rapid crystallisation of amorphous WS _{3+x} films: an in situ, real-time X-ray diffraction study	104

Breakthrough: using temperature-stable ZnO on poly-Si thin film solar cells

F. Ruske, C. Becker, K.Y. Lee, S. Gall, B. Rech

■ Helmholtz-Zentrum Berlin für Materialien und Energie

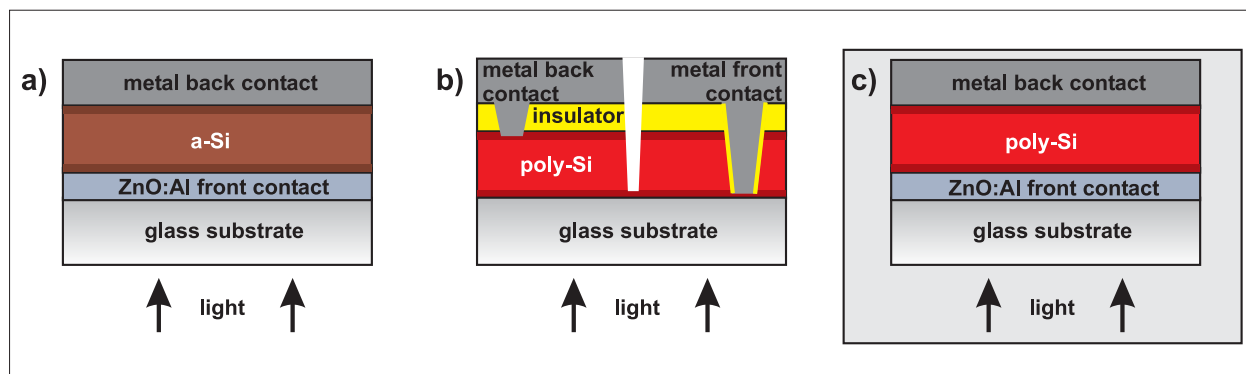


Fig. 1: Structures of state-of-the-art silicon thin film solar cells: a) based on amorphous silicon (a-Si) using a ZnO:Al layer as transparent conductive front contact; b) based on polycrystalline silicon (poly-Si) with the front contacts etched from the rear side (CSG Solar); c) HZB's approach combining both a ZnO:Al front contact layer and high-quality poly-Si produced at high temperatures.

Solar cell contacts are a key issue determining cell efficiency. Contacts have to be applied to both ends of the p-/n-junction of a cell and are usually classified as front or back contacts, depending which side of the solar cell is irradiated with light.

In thin film solar cell technology, the front contact usually consists of a transparent, conducting layer, normally highly doped zinc oxide (ZnO:Al) or tin oxide. Such layers are widely used for thin film silicon solar cells based on amorphous silicon (Figure 1a). In this type of cell the absorber material is deposited at quite low temperatures of about 200°C onto a cheap transparent substrate (e.g. glass), coated with a transparent conducting oxide (TCO) layer. This layer allows the light to enter the absorbing amorphous silicon (a-Si) while the electrical current can be conducted over substantial lateral distances. Due to the high conductivity of these layers resistive losses are still negligible for collection areas with a breadth of several millimetres. Several solar cells of this size can be produced in a series connection by a laser scribing process.

Apart from these advantages, the front contact can also be used to improve the light collection of the cells as the TCO layer reduces cell reflection and can also be used to scatter light into the solar

cell, effectively lengthening the light path through the absorber.

Thin film solar cells based on polycrystalline silicon (poly-Si) exhibit the potential for very high material quality and thus better cell efficiency. However, up to now, they have usually been produced without a TCO layer on the substrate, as at some stage in the fabrication process the production of poly-Si requires high temperature treatment which could destroy the TCO layer. At CSG Solar, currently the only company producing poly-Si on a large scale, an annealing step at around 600 °C is applied for several hours.

In order to contact the junction, which is then buried, local wet chemical etching is used to remove parts of the absorber layer, and subsequently contacts are deposited onto the exposed areas (Figure 1b). CSG Solar has developed a sophisticated procedure in which these contacts are formed as point contacts, allowing a series connection of individual cells on large substrates [1].

The present work at HZB aims at combining poly-Si solar cells, offering the potential for high single junction efficiency, with a TCO layer made up of aluminium doped zinc oxide (ZnO:Al) to contact the solar cell from the glass side (Figure 1c). For this approach to be successful it is essential that the zinc oxide layer maintains its high conductiv-

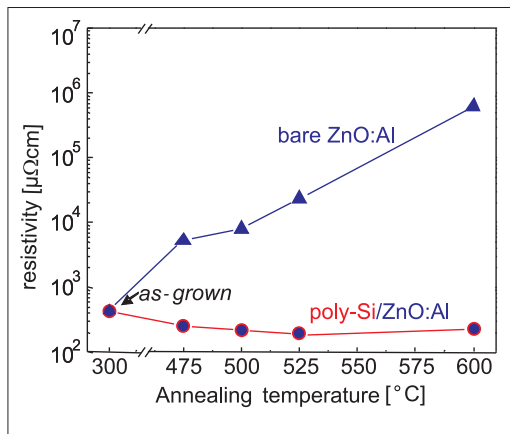


Fig. 2: The resistivity ρ of glass/ZnO:Al/poly-Si (circles) and glass/ZnO:Al (triangles) as a function of the annealing temperature. For all data points up to 525°C the poly-Si films were produced by aluminium-induced crystallisation [4], while the film at 600°C was produced by thermal crystallisation of amorphous silicon.

ity (low resistivity) throughout the thermal treatment needed for poly-Si formation.

In a series of experiments the effect of several hours of thermal treatment on the resistivity of various layer stacks was examined. The resistivity of bare ZnO:Al films on glass was found to degrade quickly compared to the as-grown value (Figure 2, triangles) a finding which had already been documented [2]. By annealing at 600 °C for 24 hours the resistivity was even found to increase by more than three orders of magnitude.

By contrast, the resistivity of the ZnO:Al films coated with silicon is even lower than the resistivity of the as-grown ZnO:Al layer (Figure 2, circles). We ascribe this to an improvement in ZnO:Al quality, as the silicon does not contribute to the total resistance of the stack to any extent. The resulting resistivity of the glass/ZnO:Al/poly-Si samples is almost unaffected by the annealing temperature. Hence, the silicon layer on top of the ZnO:Al effectively prevents the degradation by oxygen or nitrogen [3]. In the case of the samples annealed at 600°C for 24 hours the resistivity of the covered ZnO:Al films dropped from $(4.3 \pm 0.1) \cdot 10^2 \mu\Omega\text{cm}$ to a value of $(3.4 \pm 0.1) \cdot 10^2 \mu\Omega\text{cm}$. This is a very promising result regarding the application of sputtered ZnO:Al layers in poly-Si thin-film solar cells. The first poly-Si thin film solar cells on ZnO:Al layers were prepared at HZB [5] using high-temperature steps up to 600°C without degradation of the conductivity of the ZnO:Al front contact film.

In conclusion, it was found that the electrical properties of aluminium doped zinc oxide (ZnO:Al) layers remain stable during heat treatment if they are covered by a thin silicon film. These ZnO:Al layers withstand annealing temperatures and times which are typical for poly-Si thin-film fabrication. This means that ZnO:Al thin films can be used as transparent conductive front contact for poly-Si solar cells.

- [1] M.A. Green, P.A. Basore, N. Chang, D. Clugston, R. Egan, R. Evans, D. Hogg, S. Jarnason, M. Keevers, P. Lasswell, J. O'Sullivan, U. Schubert, A. Turner, S.R. Wenham, and T. Young, *Solar Energy* 77, 857 (2004)
- [2] T. Minami, T. Miyata, and T. Yamamoto, *J. Vac. Sci. Technol. A* 17, 1822 (1999)
- [3] K. Y. Lee, C. Becker, M. Muske, F. Ruske, S. Gall, B. Rech, M. Berginski, and J. Hüpkes, *Appl. Phys. Lett* 91, 241911 (2007)
- [4] S. Gall, J. Schneider, J. Klein, K. Hübener, M. Muske, B. Rau, E. Conrad, I. Sieber, K. Petter, K. Lips, M. Stöger-Pollach, P. Schattschneider, and W. Fuhs, *Thin Solid Films* 511-512, 7 (2006)
- [5] C. Becker, E. Conrad, P. Dogan, F. Fenske, B. Gorka, T. Hänel, K. Y. Lee, B. Rau, F. Ruske, T. Weber, M. Berginski, J. Hüpkes, S. Gall, and B. Rech, *Sol. Energy Mat. Sol. Cells*, (2008)

Photoconductivity in Single Si/SiO₂ Quantum Wells

Bert Stegemann, Thomas Lussky, Andreas Schoepke, Manfred Schmidt

■ Helmholtz-Zentrum Berlin für Materialien und Energie Berlin, Germany

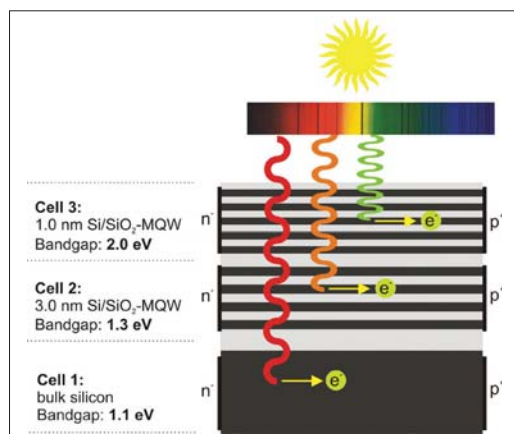


Fig. 1: Conceptual design of an all-Si tandem cell, based on Si/SiO₂ multiple QW superlattices. Two solar cells of different energy bandgaps controlled by QW thickness are stacked on top of a c-Si cell.

Introduction

The major loss factor in conventional solar cells is the thermalisation of hot charge carriers generated by photons with energies exceeding the bandgap energy. Third-generation photovoltaic science aims to significantly increase conversion efficiency by circumventing these thermalisation losses. A promising concept explored by our group is the use of multiple absorbers consisting of Si/SiO₂ multiple quantum wells (QWs), in order to provide energy bandgap tunability via the utilisation of quantum size effects and thus adaptation to the solar spectrum. The conceptual design of such a photovoltaic device is shown in Figure 1: two solar cells of different bandgaps controlled by the QW thickness are stacked on top of a third c-Si cell, so that each stack is able to absorb a different part of the solar spectrum. The basic building block of such superlattices is a single QW. Thus, the present study focused on the well-defined preparation of SiO₂/Si/SiO₂-QWs and the analysis of their properties, in order to provide a gateway to the enhancement of solar cell efficiencies by the utilisation of quantum size effects.

Method

Basically, Si/SiO₂ single QWs were prepared under ultrahigh vacuum conditions in four sequential

steps: [1] deposition of ultrathin, initially amorphous Si layers onto clean 2" SiO₂ substrates, [2] RF plasma oxidation with thermalised, neutral oxygen atoms at 600°C, [3] crystallisation by thermal annealing at 1000°C, [4] interface passivation by hydrogen treatment. After preparation, the samples were analysed by photoelectron spectroscopy with either x-ray excitation (XPS, 1253.6 eV) or near-UV light excitation (NUV-PES, 6.5 eV). XPS analysis of the chemical shift of the Si2p core level electrons was used to identify interface stoichiometry and NUV-PES was applied to analyse electronic gap state densities at the SiO₂/Si interface. For photoconductivity (PC) measurements, coplanar Ohmic contacts were prepared and the samples were illuminated with monochromatic light of variable photon energy and intensity.

Results and Discussion

The cross-sectional TEM image (inset Fig. 2) shows a typical Si single QW with a homogeneous thickness of ~7 nm, which is covered by a ~2 nm thick SiO₂ barrier. Within the Si layer, lattice planes are clearly visible, indicating a high degree of crystalline order. As evidenced by XPS (Figure 2), the formation of suboxides is highly suppressed by RF plasma oxidation and abrupt Si/SiO₂ interfaces are formed. These physical features are essential prerequisites for the envisaged realisation of Si/SiO₂ superlattices with varying periodicity.

Photoelectrical properties were explored by the analysis of the spectral dependence of the lateral photocurrent, since lateral transport (i.e. parallel to the Si/SiO₂ interfaces of a multi-QW structure) has been demonstrated to be four orders of magnitude more efficient compared to vertical transport across the stack. Figure 3a shows the spectral dependence of the internal quantum efficiency of photoconductivity ($Y_{\text{int,PC}}$) for the 7 nm QW. It is evident that even in such ultrathin Si layers a photocurrent can be detected. The onset of the dominant part occurs in the energy range of the direct c-Si bandgaps at 3.6 and 4.2 eV. From $Y_{\text{int,PC}}$ a mobility-lifetime-product ($\mu\tau$) of about $1 \times 10^{-8} \text{ cm}^2 \text{V}^{-1}$ is estimated, and this rather low value suggests a strong influence of Si/SiO₂ interface states on the carrier mobility and lifetime in Si QWs.

Studies on hydrogen passivation revealed a considerable improvement of the photoelectrical performance, resulting in an increase in $Y_{\text{int,PC}}$, and

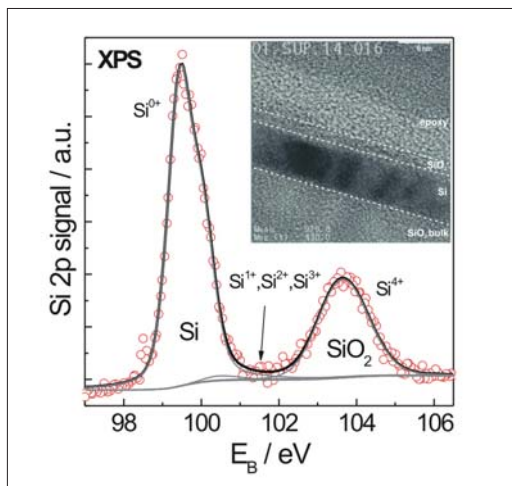


Fig. 2: XPS analysis of the chemical shift of the Si2p signal. Inset: cross-sectional high-resolution TEM image of the Si/SiO₂ single QW.

thereby of $\mu\tau$, by a factor of 10 upon treatment in forming gas (Figure 3a). NUV-PES revealed that this effect is due to the passivation of the occupied defect gap states at the interface of ultrathin SiO₂ and Si. Figure 3b shows the internal photoelectron yield ($Y_{\text{int,PES}}$) of the SiO₂/Si(111) interface before and after in situ plasma passivation with hydrogen atoms at nearly thermal impact energies, which turned out to be even superior to forming gas treatment. There is a distinct decrease in $Y_{\text{int,PES}}$ particularly around the midgap, where dangling bonds are located. Since, at a first approximation, $Y_{\text{int,PES}}$ is proportional to the number of occupied states, it is concluded that this hydrogen treatment efficiently passivates dangling bonds at the SiO₂/Si interfaces as well as at grain boundaries inside the nc-Si layers of the QWs. Moreover, it has been shown that the increase in $\mu\tau$ (due to dangling bond passivation) is accompanied by a reduction of interface recombination velocity and an increase in effective majority and minority carrier lifetimes, as revealed by constant photocurrent measurements and quasi-steady-state PC respectively.

Summary and Outlook

Si/SiO₂ single-QWs were successfully prepared and studied with respect to possible photovoltaic applications. The presence of a photocurrent in such structures was demonstrated. Internal quantum efficiencies and carrier lifetimes are strongly affected by Si/SiO₂ interface recombination and were enhanced upon hydrogen passivation. These results are promising, but still require substantial improvement before photovoltaic devices based on Si/SiO₂ quantum structures can become widespread in their application.

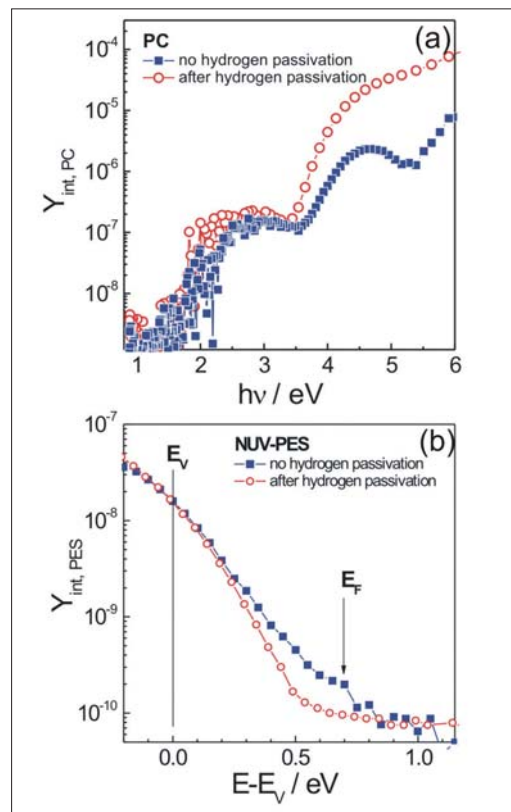


Fig. 3: (a) Spectral dependence of the internal quantum efficiencies of photoconductivity ($Y_{\text{int,PC}}$) of a 7 nm Si/SiO₂ single QW, shown on a logarithmic scale. (b) Internal yield from NUV-PES measurements. E_F = Fermi energy, E_V = valence band maximum.

- [1] B. Stegemann, A. Schoepke, M. Schmidt, *J. Non-Cryst. Sol.* 354 (2008) 2100.
- [2] B. Stegemann, D. Sixtensson, T. Lussky, U. Bloeck, M. Schmidt, *Chimia* 61 (2007) 826.
- [3] L. Korte, M. Schmidt, *J. Non-Cryst. Sol.* 354 (2008) 2138.
- [4] R. Röfver, B. Berghoff, D. Bätzner, B. Spangenberg, H. Kurz, M. Schmidt, B. Stegemann, *Thin Solid Films* 516 (2008) 6763–6766.
- [5] B. Stegemann, D. Sixtensson, T. Lussky, A. Schoepke, I. Didschuns, B. Rech, M. Schmidt, *Nanotechnology* 19 (2008) 424020.
- [6] B. Stegemann, A. Schoepke, D. Sixtensson, B. Gorka, T. Lussky, M. Schmidt, *Physica E* (2009) doi:10.1016/j.physe.2008.08.012.

Corresponding author:

B. Stegemann
bert.stegemann@helmholtz-berlin.de

Room temperature electrical detection of spin coherence in C_{60}

W. Harnett^{1,2}, C. Boehme^{2,3}, S. Schäfer^{1,2}, K. Hübener¹, K. Fostiropoulos², K. Lips²

■ 1 Freie Universität Berlin, Institut für Experimentalphysik, Arnimallee 14, 14195 Berlin

■ 2 Helmholtz-Zentrum Berlin für Materialien und Energie, Berlin, Germany

■ 3 Department of Physics, University of Utah, 115 S 1400 E, Suite 201, Salt Lake City, Utah 84112-0830, USA

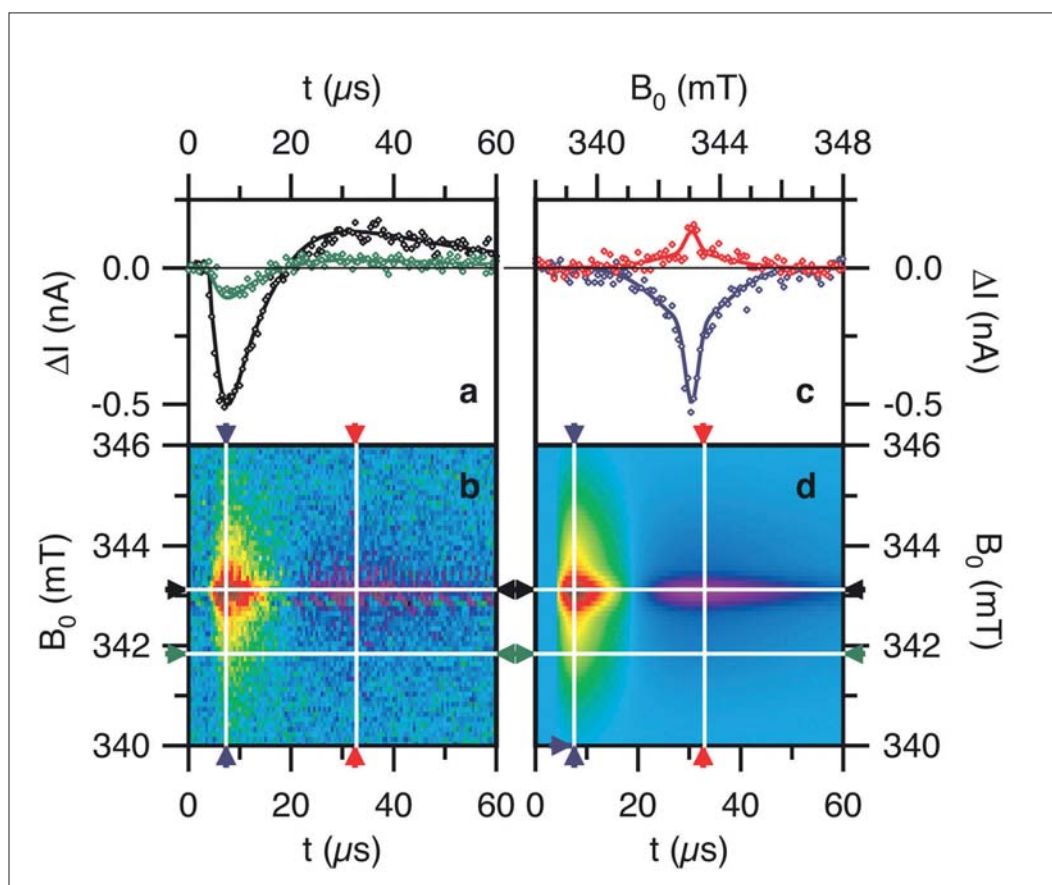


Fig. 1: Transient current ΔI of a C_{60} film illuminated with a halogen lamp, after a microwave pulse. Time traces (a) were recorded at different magnetic fields B_0 to afford the 2D dataset (b). 1D cuts along the field dimension (c) reveal the spin-resonant behaviour. Panel (d) displays a global fit of the data in (b) and markers indicate where the cuts in (a) and (c) were taken (lines = fit, symbols = data).

Spin dynamics and spin coherence in organic materials are of fundamental interest in the applications of organic semiconductors in spintronics [1] and quantum information processing [2], but also in organic photovoltaics. The new method of pulsed electrically detected magnetic resonance (pEDMR) recently developed at SE1, Hahn-Meitner-Institut [3], has been applied here for the first time to thin films of C_{60} fullerenes, an indispensable material for organic photovoltaics [4]. In the field of spintronics and quantum informa-

tion processing, spin-coherent effects are expected to be sufficiently long-lived only at low temperature. However, we have shown that spin coherence does prevail in this situation even at room temperature [5]. This is due to the fact that, in some sense, organic solids still retain their molecular character. Here, it means that localised electronic (or polaronic) states are often spread out over a few molecules, so that the spin degree of freedom retains the long coherence times well-known for individual molecules.

With our measurements, we detected spin resonance in the photocurrent through thin film devices by way of an ordinary electron spin resonance (ESR) setup that had been equipped with a fast current amplifier [3]. The charge carriers in organic materials are polarons (electrons associated with a surrounding local lattice deformation) that are easily trapped in the often disordered semiconductor matrix. Carrier transport (e.g. hopping) and carrier recombination obey spin selection rules: e.g. P+/P- polaron recombination is fast for spin singlet pair states but slow for triplet pair states. When the organic film is illuminated with an ordinary halogen lamp, a surplus of spin triplet states are therefore generated in the steady state. By placing the sample in a magnetic field and applying resonant microwaves, some of the triplets can be converted into singlets and will undergo fast recombination. We therefore detected a resonant photocurrent quenching as shown in Figure 1.

Spin coherence is evidenced by the fact that the triplet-to-singlet conversion efficiency depends on the length of the microwave pulse in an oscillatory manner. This can be understood as an oscillation of the triplet character, of the polaron pair's wave function. The length of the microwave pulse is proportional to the turning angle φ of the quantum mechanical phase. At $\varphi = (2n + 1)\pi$, the triplet-to-singlet conversion is maximal, whilst at $\varphi = (2n)\pi$, the original spin pair wave function is restored and no conversion has occurred.

An analysis of the oscillation frequency leads to the assignment of the spin resonance to only one of the polaron pair's spins. A comparison of line width and resonance position (or g factor) with the ESR literature on molecular spin states in C_{60} , leads to the identification of the signal with that of a positive polaron (molecular cation C_{60}^+) rather than with that of a negative polaron. The latter is much more mobile and thus likely to be subject to faster decoherence. This assignment is not unambiguous and it has been suggested in the literature that direct C_{60} - C_{60} or 'bridged' C_{60} -O- C_{60} dimers, an ubiquitous impurity in C_{60} films, may be at the origin of this spin resonance. This is in line with our observation that the intensity of the spin signal for separately prepared C_{60} thin films varies considerably even if the total photocurrent is similar.

Our results indicate that spin coherence is present at room temperature in polaronic C_{60} states and therefore, we have begun a more systematic study of this phenomenon in other relevant organic materials and in organic solar cell devices. The goal is to develop a new technique to

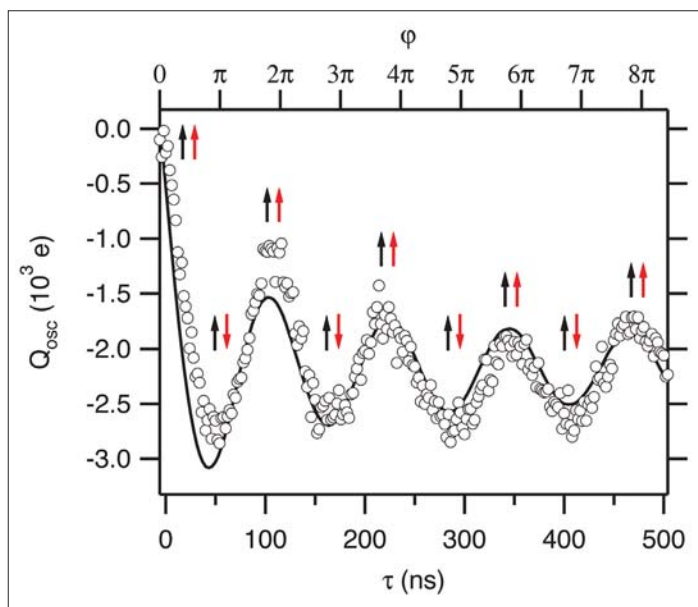


Fig. 2: The oscillatory part of the time-integrated transient current change Q_{osc} (in elementary charges) as a function of microwave pulse length τ . The spin pair state is marked by arrows. The black curve is the theoretical prediction [5] for resonance of only one of the two spins (marked in red).

assess material purity, interface quality and the electronic properties of solar cell devices. This objective may become possible since the spin-dependent phenomena studied here have a direct relation to charge carrier transport and recombination, which are crucial for the efficiency of organic solar cells.

- [1] A.R. Rocha, V.M. García-Suárez, S.W. Bailey, C.J. Lambert, J. Ferrer and S. Sanvito, *Nature Materials* 4 (2005) 335-339.
- [2] W. Harneit, *Phys. Rev. A* 65 (2007) 032333.
- [3] C. Boehme, K. Lips, *Phys. Rev. Lett.* 91 (2003) 246603.
- [4] J. Xue, S. Uchida, B.P. Rand, S.R. Forrest, *Appl. Phys. Lett.* 85 (2004) 5757-5759.
- [5] W. Harneit, C. Boehme, S. Schaefer, K. Huebener, K. Fostiropoulos, K. Lips, *Phys. Rev. Lett.* 98 (2007) 216601; W. Harneit, K. Huebener, B. Naydenov, S. Schaefer, M. Scheloske *phys. stat. sol. (b)* 244 (2007) 3879-3884.

Corresponding author:

W. Harneit
w.harneit@fu-berlin.de

In₂S₃ buffer layers for chalcopyrite solar cells

N. Allsop, W. Braun, R. Caballero, C. Camus, Ch.-H. Fischer, S. Gledhill, M. Gorgoi, R. Klenk, T. Köhler, M. Krüger, I. Lauermann, H. Mönig, P. Pistor, F. Schäfers

■ Helmholtz-Zentrum Berlin für Materialien und Energie, Berlin, Germany

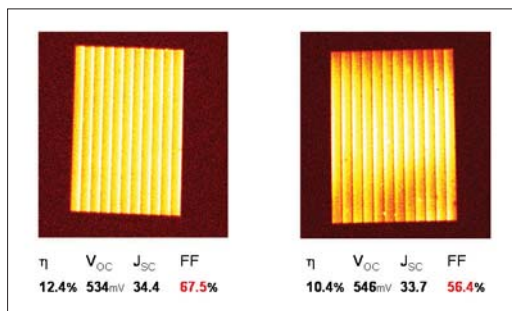


Fig. 1: Thermography and performance of two solar Cu(In,Ga)(S,Se)₂ modules with ILGAR In₂S₃ buffer. The increase in efficiency and improved homogeneity of the fill factors are evident (measured at AVANCIS).

ILGAR (Ion Layer Gas Reaction) is an alternative chemical method for the deposition of thin semiconductor layers, developed and patented¹ by HZB. This sequential, cyclic process involves spraying an aerosol containing a solution of a precursor compound, e.g. InCl₃ on a heated substrate (200-250°C). Then the sprayer is stopped and a reactant gas, e.g. H₂S is led over the solid precursor film, which is converted into the final product, e.g. In₂S₃. These two steps are repeated until the desired layer thickness is obtained.

Using industrial Cu(In,Ga)(S,Se)₂ absorbers produced by AVANCIS, a statistical comparison of the In₂S₃ buffer layers with the standard CBD-CdS buffers was made. The resulting efficiencies were absolutely comparable,² as was the stability in accelerated aging tests. ISE Freiburg has certified efficiency of 14.7% for the indium sulfide buffer, which is a very high value for an industrial absorber based cell. A more recent nanostructured ZnS/In₂S₃ buffer reached 15.3%. Additionally, the ILGAR buffer process is very robust with broad parameter windows.

A chamber for 10x10 cm² substrates moving over a linear spray nozzle was designed and constructed in house. It demonstrates the easy up-scaling of the process. Figure 1 shows a thermography test of two minimodules revealing that ILGAR buffered modules are homogenous and free of shunts.

Currently, we are working on the buffer deposition on 10 cm wide steel tape in a continuous process. Here, the material yield is clearly superior to the standard CBD process. The In conversion has al-

ready been increased to over 30 %. Moreover, the In-recycling is easier due to the lack of by-products, and production speeds should be much higher.

The Spray-ILGAR process can be integrated very easily in an industrial in-line process. CIS-Solartechnik GmbH produces Cu(In,Ga)Se₂ solar devices roll-to-roll on steel foil. They chose the ILGAR buffer because of its in-line compatibility, and the process has been successfully integrated into a pilot line. Currently, full production is being planned and a licence contract with HZB has been concluded.

A new collaboration has begun with Stangl Semiconductor Equipment, one of the leading suppliers of wet-chemical equipment for the PV-industry, including equipment for the CBD-CdS buffer layers. Impressed by the advantages of the ILGAR process and the solar cell results with Cd-free ILGAR buffers, the company is now developing industrial ILGAR coaters in cooperation with HZB which should be available commercially in 2009. Stangl will market the ILGAR buffer coaters with the HZB ILGAR process worldwide.

Another approach follows the deposition of In₂S₃ buffer layers by thermal evaporation from the compound In₂S₃. This vacuum deposition method offers full in-line compatibility for module production where the back contact, absorber and window layer are also applied by vacuum methods (e.g. co-evaporation and sputtering.) In this case, the In₂S₃ is deposited onto the cold absorber before completing the solar cell with the ZnO window layer and contacts.

Cells fabricated in this way show only comparatively low efficiencies of approximately 8-10% in the as-grown state. This changes if the completed solar cells are heated to a temperature of 200°C in air. The cell efficiency increases significantly upon annealing -mainly due to increases in the open circuit voltage and fill factor - and reaches values of more than 15% after 35-45 minutes. One of the best cells produced with an Cu(In,Ga)Se₂ absorber from the HZB baseline and an evaporated In₂S₃ buffer layer was certified by Fraunhofer ISE, Freiburg, at 15.2% .

In order to understand the effect of the annealing step, several experiments were carried out before and after annealing. We found an increase in the copper content inside the buffer layer after anneal-

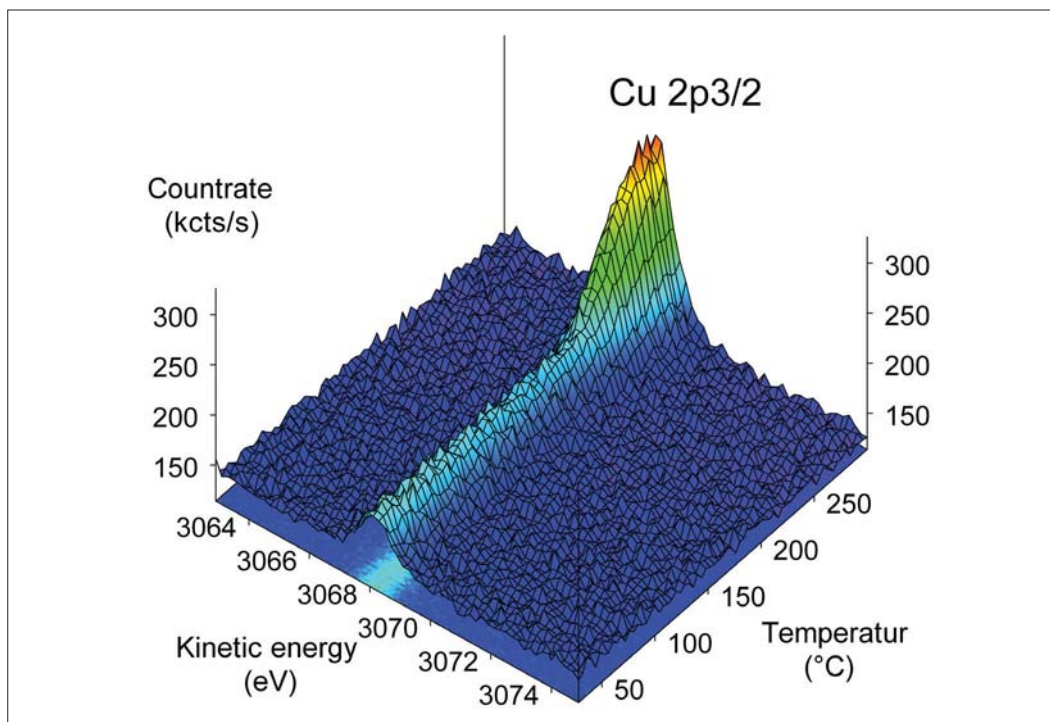


Fig. 2: Development of the high kinetic energy XPS signal of the Cu $2p^{3/2}$ peak during heat up. At the beginning only a small signal from the Cu(In,Ga)Se₂ can be detected through the 20 nm In₂S₃ covering layer. Above 200°C Cu starts to diffuse significantly into the In₂S₃ layer and the XPS signal increases.

ing and tried to demonstrate the Cu diffusion into the buffer layer. For this purpose we took advantage of a new tool at BESSY, the HIKE endstation (High Kinetic Energy X-ray photoelectron spectroscopy). This tool offers the opportunity to detect photoelectrons with high kinetic energy of up to 10keV induced by a high resolution and high flux synchrotron beam on the BESSY KMC-1 beamline. The use of higher excitation energies results in high kinetic energy and an increase in the escape depth of the resulting photoelectrons. This vastly extends the information depth by comparison with standard XPS, and photoelectrons can be detected even through cover layers of up to a few tens of nanometres.

In our experiment we used a Cu(In,Ga)Se₂ absorber from the HZB baseline and deposited a 20nm In₂S₃ layer on top of it. The absence of a Cu signal for excitation energies $E_{exc} < 4000$ eV indicated a closed In₂S₃ layer, while for $E_{exc} > 4000$ eV a low intensity Cu $2p^{3/2}$ signal was detectable through the In₂S₃ layer. At 4000 eV, Cu 2p spectra were recorded continuously while heating the sample up to 300° C. The results are presented in Figure 2. The interdiffusion of the Cu from the absorber into the In₂S₃ layer is clearly indicated by an increase in the Cu signal at temperatures above approximately 200° C. This interdiffusion and the corresponding changes at the In₂S₃/Cu(In,Ga)Se₂

interface are probably the key to the increase in the performance of solar cells after annealing and will be addressed in future work.

Acknowledgement: The authors would like to thank Dr. T. Niesen (AVANCIS GmbH, Munich) for the Cu(In,Ga)(S,Se)₂ absorbers and the measurements on the minimodules.

- [1] Fischer, Ch.-H.; Lux-Steiner, M. Ch.; Möller, J.; Könenkamp, R.; Siebentritt, S.: "Verfahren und Anordnung zur Herstellung dünner Metallchalkogenid-Schichten", German Patent 198 31 214.8 and various Internat. Patents.
- [2] N. A. Allsop, A. Schönmann, H.-J. Muffler, M. Bär, M. C. Lux-Steiner and Ch.-H. Fischer, "Spray-ILGAR Indium Sulfide Buffers for Cu(In,Ga)(S,Se)₂ Solar Cells", Prog. Photovolt: Res. Appl. 2005; 13:607–616
- 1 P. Pistor, et al., accepted for Sol. Energy Mater. Sol. Cells (2008), doi:10.1016/j.solmat.2008.09.015
- 2 P.Pistor, et al., "Cu in In₂S₃: interdiffusion phenomena analysed by high kinetic energy X-ray photoelectronspectroscopy", submitted to physica status solidi, October 2008

Corresponding author:

Christian-Herbert Fischer
fischer@helmholtz-berlin.de

Beyond conventional thin films: growth and characterisation of chalcopyrite nanocrystals

D. Fuertes Marrón^{1,2}, S. Lehmann¹, J. Kosk³, S. Sadewasser¹, and M.Ch. Lux-Steiner¹

■ 1 Helmholtz-Zentrum Berlin für Materialien und Energie Berlin, Germany ■ 2 Instituto de Energía Solar – ETSIT, Universidad Politécnica de Madrid, Avd. Complutense s.n., 28040 Madrid, Spain ■ 3 Gdansk University of Technology, Danzig, Poland

Introduction

Devices based on Cu-containing chalcopyrite absorbers, with efficiencies around 20 % [1], are currently state of the art in thin-film solar cell technology. In addition to their application in thin film solar cells, chalcopyrites have unique properties, like high absorption coefficients, complex valence band structures, forgiving defect chemistries that also make them interesting for other branches of microelectronics, including sensors, spintronics and non-linear optical devices. In these fields, patterning and lateral structuring at reduced dimensions is commonplace. Even within the field of photovoltaics, the possibility of implementing high-structuring schemes of active materials might be of relevance. For these reasons, it is expected that the development of strategies aiming at the growth of highly structured material will become relevant for new applications, and in turn, widen the potential applications of chalcopyrites beyond standard PV-devices. Additionally, the study of complex structures can provide further knowledge on the basics of growth mechanisms, as well as the structural and electronic properties of chalcopyrite materials.

In view of this, we developed a method for the growth of laterally structured chalcopyrite materials of the $\text{Cu}(\text{In,Ga})(\text{S,Se})_2$ type based on the deposition of metal precursors [2-4]. When the set of processing parameters are properly selected, nanocrystals and sub-micrometre polycrystalline dots can be grown in this way, either as isolated units or, alternatively, as embedded structures in a matrix of a binary chalcogenide compound. General investigations of the growth process and characterisation by scanning probe techniques have been performed.

Experiment

The growth of highly structured semiconducting material was considered as a two-fold problem: i) the structuring, i.e. the ability to control the shape and size during the deposition process of the material; ii) the chemistry, i.e. the growth of high-quality material. In order to accomplish both conditions, we opted for a sequential process: 1) the use of metallic precursors deposited on standard

Mo-coated glass substrates by evaporation or sputtering to control the structuring, ranging from nanoparticles, macroscopic clusters, or semi-transparent ultra-thin-films; 2) the use of chemical vapour deposition (CVD) as the exemplary reaction process for obtaining the target compounds to control the chemistry. As a precursor, Cu was used in two different forms:

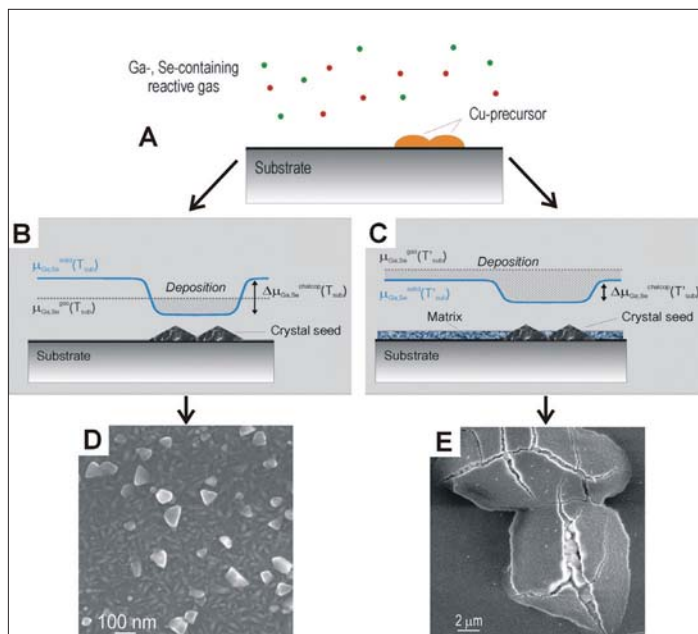
- Cu-nanoparticles were evaporated onto Mo-coated glass substrates. The evaporation process was only run for a few seconds in order to provide a fairly random distribution of Cu particles of nanometre-size, but avoid the formation of a closed Cu overlayer.
- Macroscopic Cu-dots were evaporated using a mask in the form of dots with $500\mu\text{m}$ diameter and some 200 nm thickness.

The substrates with the Cu-precursor were subsequently introduced into an open-tube CVD reactor and were exposed to a reactive gas atmosphere containing Ga and Se in the form of metal halide and H_2Se [5]. Scanning probe techniques, namely scanning electron microscopy (SEM), atomic force microscopy and scanning tunnelling microscopy, were used for the characterisation of the structures [2,3].

Results And Discussion

As for any conventional CVD-based process, the effective volatilisation and deposition of material for given temperature T and pressure p can be satisfactorily explained by the unbalance of the chemical potentials μ (molar free energies) of the different species contained in the gas and the solid phases, according to $\Delta\mu = \mu_{\text{gas}} - \mu_{\text{solid}}$ (Figure 1 A-C). For $\Delta\mu > 0$, deposition from the gas continues into the solid phase and for $\Delta\mu < 0$, the reaction is perpetuated into the gas phase. The presence of finite precursors on the substrate exposed to the reactive gas introduces lateral variations in the chemical potential inequalities. These variations are responsible for the selective deposition into the solid phase of both the isolated structures at the spots where the precursor is located (Figure 1 B) or, alternatively, for the simultaneous occurrence of reactions into the solid phase *at* and *off* the precursor (Figure 1 C). The result of such pro-

Fig. 1: A: Schematics of the general method employed for the growth of chalcopyrite nanocrystals. The size and distribution of metal precursor particles determine the size and distribution of the crystallites. B: For a given pressure p and temperature T_{sub} , the condition for the growth of isolated clusters of ternary compound relate locally to the precursor for net deposition (hatched area). C: The conditions for the growth of chalcopyrite dots embedded in a matrix formed from the elements contained in the gas phase are shown in C. Local differences still exist for the different solid phases that do or do not contain the precursor as constituent. D: SEM top view of isolated CuGaSe_2 nanocrystals grown onto Mo-coated glass. E: SEM top view of CuGaSe_2 structures embedded in Ga_2Se_3 after a single reaction process.



cesses is the formation of chalcopyrite structures, either as isolated or as embedded structures in a matrix of a different semiconducting compound. Under the growth conditions at the CVD reactor, the critical parameter governing the switch from one process to the other was the substrate temperature, which can easily be adjusted even during the process.

Single-phase isolated CuGaSe_2 nanocrystals were grown on Mo-coated glass from Cu-precursors of nm-size by exposing the precursors to GaCl_x and H_2Se reactants at a substrate temperature $T_{\text{sub}} = 530^\circ\text{C}$ (Figure 1 D). The growth of semiconductor material takes place at the spots where the Cu-precursor is present, as confirmed by compositional studies *at* and *off* the crystallites.

The adjustment of processing parameters allows the isolated structures to be embedded in a matrix of a binary semiconductor during a single processing step, as shown in Figure 1 E. In this case, CuGaSe_2 crystals grown onto Mo-coated glass substrates appear to be covered by a thin Ga_2Se_3 overlayer that probably fractured during fast cooling down due to thermal stress. At the crack, the embedded structures are visible. Similar, crack-free structures have been grown with macroscopic clusters and tiny nanocrystals embedded in them.

The possibility of forming self-assembled semiconductor heterojunctions in a single process is a clear advantage in comparison with alternative methods. A typical tuned process combines a short reaction time at higher temperatures (aiming at the formation of the embedded target material), with a lower temperature last stage, providing the homogeneous coating and more or

less inhibiting further reactions between embedded and embedding phases.

Acknowledgments

The authors would like to thank M. Kirsch, S. Wiesner, M. Hafemeister, and J. Albert for technical support and Dr. Ch. A. Kaufmann for SEM/EDX analysis.

- [1] I. Repins, M.A. Contreras, B. Egaas, C. DeHart, J. Scharf, C.L. Perkins, B. To and R. Noufi, *Prog. in Phot.: Res. and Appl.* 16, 235, (2008)
- [2] D. Fuertes Marrón, S. Lehmann, J. Kosk, S. Sadewasser, M.Ch. Lux-Steiner, in *Thin-Film Compound Semiconductor Photovoltaics—2007*, edited by T. Gessert, K. Durose, C. Heske, S. Marsillac, T. Wada (Mater. Res. Soc. Symp. Proc. Vol. 1012, Warrendale, PA, 2007), pp. Y02-07.
- [3] D. Fuertes Marrón, S. Lehmann, and M.Ch. Lux-Steiner, *Phys. Rev. B* 77, 085315 (2008).
- [4] D. Fuertes Marrón, S. Sadewasser, S. Lehmann, and M.Ch. Lux-Steiner, patent pending.
- [5] D. Fuertes Marrón, A. Meeder, R. Würz, S.M. Babu, M. Rusu, Th. Schedel-Niedrig, and M.Ch. Lux-Steiner, in *Proc. Int. Conf. PV in Europe - From PV technology to energy solutions*, 7-11 October 2002, Rome, Italy, edited by WIP Munich-ETA Florence, pp. 421-424 (2002), and references therein.

Corresponding author:

Sascha Sadewasser
sadewasser@helmholtz-berlin.de

Solar cells based on ZnO nanorod arrays with extremely thin sulphide absorber

Th. Dittrich, A. Belaidi, D. Kieven, J. Tornow, K. Schwarzburg, N. Allsop, M. Rusu, M. Kunst, J. Chen, L. A  , M. Lux-Steiner

■ Helmholtz-Zentrum Berlin f  r Materialien und Energie, Berlin, Germany

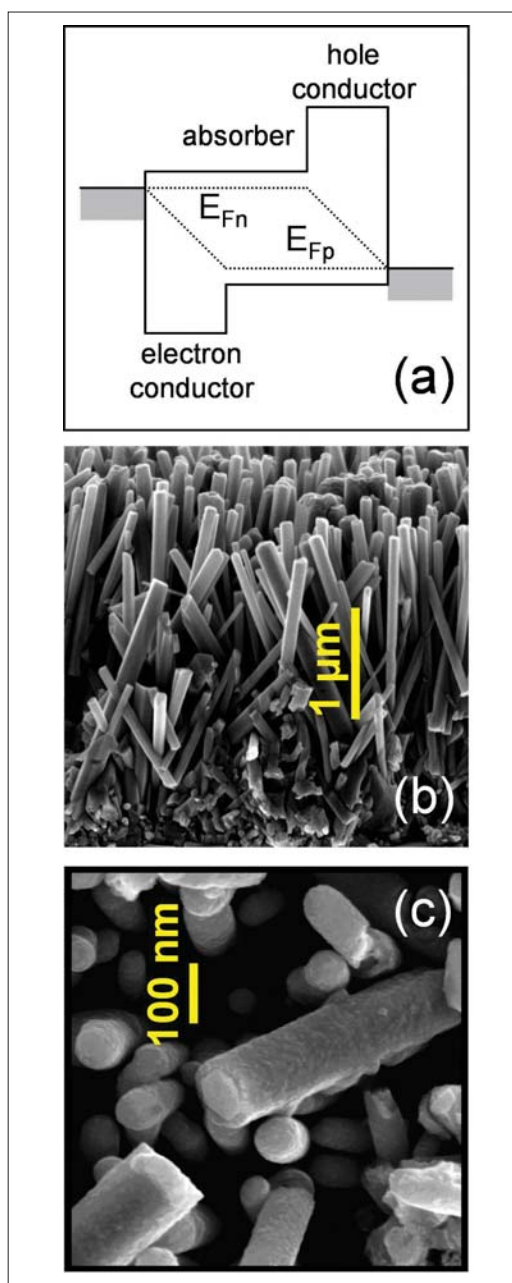


Fig. 1: (a) Idealised local band diagram under illumination. (b) Cross section view of a ZnO nanorod array prepared chemically. (c) Cross section view of a broken ZnO nanorod coated with In₂S₃.

The extremely thin absorber concept

By using nanostructured materials as contacts and absorbers, solar cells with extremely thin absorber (eta) offer the possibility of low-cost solar cells with high efficiency. The eta-concept is based on the high optical density of inorganic absorber layers with a low diffusion length of photo-generated charge carriers (L_{diff}). The absorber is sandwiched between transparent electron and hole conductors (Figure 1). The interface area between the electron and hole conductors is increased by structuring, in order to increase the effective absorber layer thickness and also to incorporate measures of photon management or light trapping [1]. The *local* thickness of the absorber layer (d_{local}) should be less than L_{diff} but larger than the tunneling length (l_{tunn}). This limits d_{local} to the order of tens of nm which is usually significantly lower than the absorption length of the absorber (α^{-1}). Therefore, the absorber has to be folded to reach an effective absorber layer thickness (d_{eff}) which is significantly larger than α^{-1} . The roughness factor (K) is defined as the ratio d_{eff}/d_{local} . In a theoretical model, it has been shown that efficiencies of up to 15% could be reached with d_{local} between 15 and 20 nm and L_{diff} and K being in the order of 10 nm and 10, respectively [2]. For proof of this concept, we developed a model system consisting of ZnO/In₂S₃/In₂S₃/Cu/CuSCN to investigate the roles of interface formation, d_{local} and d_{eff} .

ZnO nanorod arrays as a structured electron conductor

ZnO nanorods were prepared chemically in a chemical bath (CBD) or electrochemically. Figure 1(b) shows an example of a ZnO nanorod array prepared by CBD. Well defined columns of ZnO were formed, with diameters in the range of 40 to 100 nm and lengths in the order of several μ m. In this way, K could be changed systematically between 1 and 30 [3]. The ZnO nanorods were highly n-type doped after preparation. The concentration of free electrons was decreased by annealing. The defect concentration in ZnO nanorods was greatly reduced by applying an electrochemical preparation method and in this case, the internal quantum efficiency of the photoluminescence signal of exciton recombination was very high [4, 5].

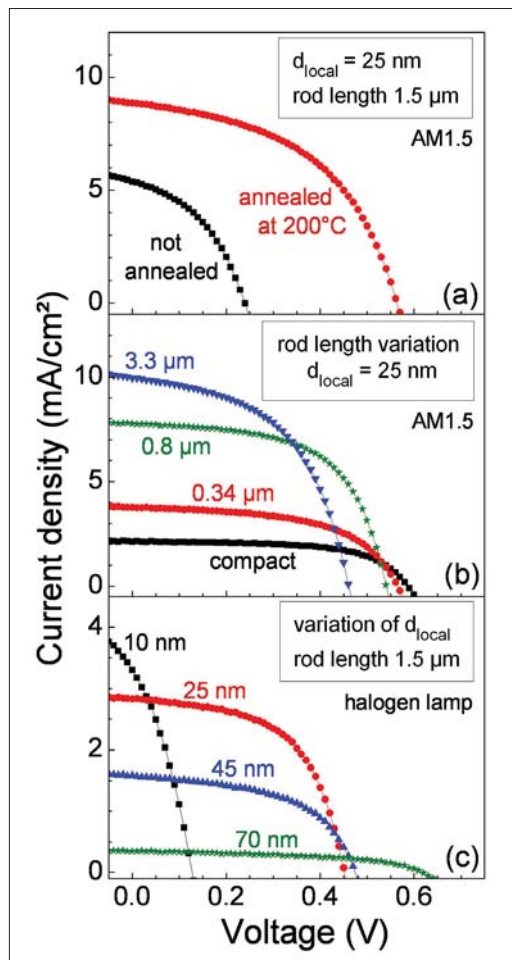


Fig. 2: Current-voltage characteristics of: (a) compact ZnO/In₂S₃/CuSCN before and after annealing at 200°C in air under illumination at AM1.5, (b) of annealed eta-solar cells with constant d_{local} and varying rod length, (i.e. d_{eff}) under illumination at AM1.5, and (c) of annealed eta solar cells with constant rod length and varying d_{local} , under illumination with a halogen lamp.

Sulphide absorber and CuSCN hole conductor

The ILGAR (ion layer gas reaction) technique was used for conformal deposition of In₂S₃ layers on ZnO nanorod arrays. The value of d_{local} was changed to between 10 and 70 nm [6]. The value of d_{eff} was controlled by XRF (x-ray fluorescence). The transparent CuSCN (band gap 3.5 eV) hole conductor was deposited by impregnation from solution. Time resolved microwave photoconductivity measurements showed that L_{diff} ranges between 20 and 30 nm for the given absorber layers and that the mobility of excess holes in CuSCN is of the same order as the mobility of excess electrons in ZnO nanorods. Small area solar cells with

Au back contacts were investigated by temperature dependent current-voltage and quantum efficiency (QE) measurements. After the annealing of the solar cells, the QE as well as the surface photovoltage signal increased in the near infrared region due to diffusion of Cu.

The roles of annealing in air and the thickness of local and effective absorber layers

The formation of the charge selective contact at the site of the hole conductor is crucial for reaching relatively high open circuit voltages (VOC). As a very good correlation between K and the short circuit current density has been demonstrated [3], and is shown in Figure 2(b). However, VOC decreases with increasing K due to increasing diode saturation current density.

Using ZnO nanorods of fixed length, the highest ISC was obtained for the lowest d_{local} (Figure 2(c)), [6]. The ISC decreases if the d_{local} is increased from 10 to 25 nm, which gives evidence for $L_{\text{diff}} < 25$ nm. At the same time, VOC increases greatly with increasing d_{local} due to a decreasing tunneling recombination.

Summary

The eta solar cell concept has been proven by using a system consisting of ZnO nanorod arrays with In₂S₃/In₂S₃-Cu absorber. The high optimisation potential for this type of solar cell has been demonstrated. At present, energy conversion efficiencies of up to about 3.6% have been reached. Future challenges include the application of alternative building blocks for absorber layers, such as nano-crystallites and quantum dots.

The project was supported by EFRE (WK-2012 / 10133711).

- [1] K. Ernst, A. Belaidi, and R. Könenkamp, *Semicond. Sci. Technol.* 18 (2003) and refs. therein.
- [2] K. Taretto, U. Rau, *Prog. Photovolt.: Res. Appl.* 12 (2004) 573.
- [3] D. Kieven, Th. Dittrich, A. Belaidi, J. Tornow, K. Schwarzburg, N. Allsop, M. Lux-Steiner, *Appl. Phys. Lett.* 92 (2008) 153107-153109.
- [4] J. Chen, L. A e, Ch. Aichele, M. Ch. Lux-Steiner, *Appl. Phys. Lett.* 92 (2008) 161906.
- [5] L. A e, J. Chen, M. Ch. Lux-Steiner, *Nanotechnol.* 19 (2008) 475201.
- [6] A. Belaidi, Th. Dittrich, D. Kieven, J. Tornow, K. Schwarzburg, M. Lux-Steiner, *phys. stat. sol. (RRL)* 2 (2008) 172-174.
- [7] Th. Dittrich, D. Kieven, M. Rusu, A. Belaidi, J. Tornow, K. Schwarzburg, M. Lux-Steiner, *Appl. Phys. Lett.* 93 (2008) 053113.

Corresponding author:

Th. Dittrich
dittrich@helmholtz-berlin.de

Electronic properties of grain boundaries in polycrystalline, chalcopyrite-type thin films in solar cells

Daniel Abou-Ras, Jürgen Bundesmann, Raquel Caballero, Christian A. Kaufmann, Jo Klaer, Melanie Nichterwitz, Roland Scheer, Thomas Unold, Hans-Werner Schock

■ Helmholtz-Zentrum Berlin für Materialien und Energie, Berlin, Germany

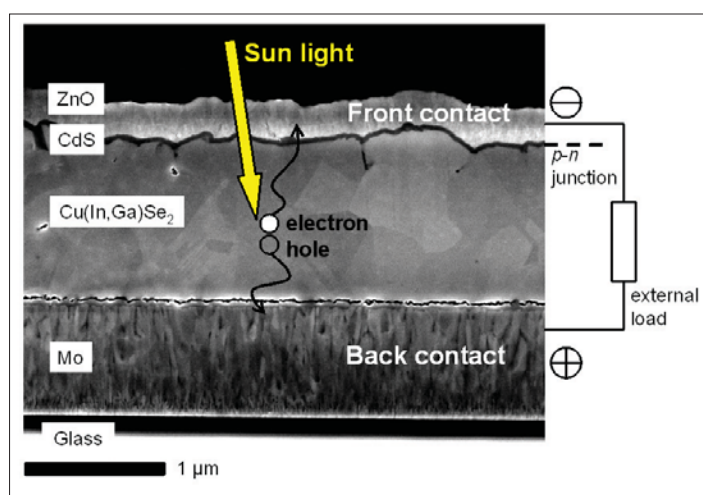


Fig. 1: Scanning electron micrograph from a Cu(In,Ga)Se_2 solar cell (cross-section), and the schematics of its mode of operation.

Thin-film solar cells based on polycrystalline, chalcopyrite-type absorbers such as Cu(In,Ga)Se_2 or CuInS_2 show the potential for high photovoltaic conversion efficiencies at low-cost. It is not yet clear why polycrystalline, chalcopyrite-type, thin-film solar cells exhibit high solar cell performances, as the grain sizes are rather small (averaging about 0.5-1 μm in diameter) and therefore the densities of grain boundaries that are expected to represent locations of enhanced losses, are rather large. The grain boundaries of CuInS_2 and Cu(In,Ga)Se_2 thin films in completed solar cells were studied by in-line electron holography in a transmission electron microscope, as well as by cathodoluminescence (CL) and electron-beam induced current (EBIC) in combination with electron backscatter diffraction (EBSD) measurements. Grain boundaries were divided into two types exhibiting different electronic activities, $\Sigma 3$ (twin) and non- $\Sigma 3$ boundaries ("random").

A scanning electron micrograph from a Cu(In,Ga)Se_2 thin-film solar cell in cross-section is shown in Figure 1. The p - n junction of the solar cell is composed of the p -type Cu(In,Ga)Se_2 and the n -type

CdS and n -type ZnO , which also acts as a transparent front contact.

EBIC and EBSD measurements acquired at this cross-section were used to investigate the influence of grain boundaries and grain boundary types on local charge collection. It was found that profiles extracted across grain boundaries from EBIC images show a small yet significant drop in the electron beam induced current for the random boundaries, whereas at the $\Sigma 3$ (twin) boundaries showed no significant contrast. Quantitative analysis of the electron beam induced current collection was performed by use of a simulation model that took account of the grain boundary recombination velocity, cross-section surface recombination velocity and the bulk diffusion length of carriers. As is shown in Figure 2, grain boundary recombination velocities of $\leq 5 \times 10^3 \text{ cm/s}$ were detected by the EBIC experiment, whereas grain boundary recombination velocities of $< 10^3 \text{ cm/s}$ did not lead to a detectable contrast. From comparison of this simulation with the experimentally detected profiles, it may be concluded that random boundaries show recombination velocities in the range of 10^4 cm/s , whereas the recombination velocities of $\Sigma 3$ (twin) boundaries can be estimated to be lower than the detection limit of 10^3 cm/s .

Complementary information about the electronic and chemical nature of grain boundaries can be extracted from TEM focus series experiments, which were performed on a comparable set of samples. From this experiment, phase distribution images of the regions around $\Sigma 3$ (twin) and random boundaries in a Cu(In,Ga)Se_2 thin film were reconstructed. From the phase distribution images, variations in the mean-inner potentials (MIPs) can be calculated (see Reference 1 for details). The MIP profiles shown in Figure 3 were extracted across $\Sigma 3$ (twin) and random boundaries and each averaged over 50 individual profiles. It can be seen that the depths of these MIP wells are much larger for the random boundary. Since the extent of the MIP well is about 2-4 nm and therefore much smaller than the estimated Debye length of about 50 nm (density of free carriers about $3 \times 10^{16} \text{ cm}^{-3}$ in Cu(In,Ga)Se_2), the phase contrast cannot be ex-

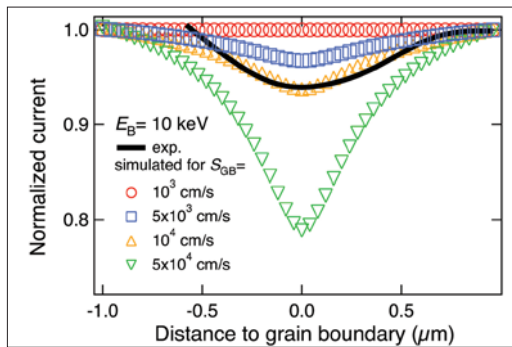


Fig. 2: Extracted EBIC profile across a random boundary (solid line) and corresponding simulations of the current for various grain boundary recombination velocities (coloured icons). The best match between experimental values and simulations is given for a recombination velocity of 1×10^4 cm/s.

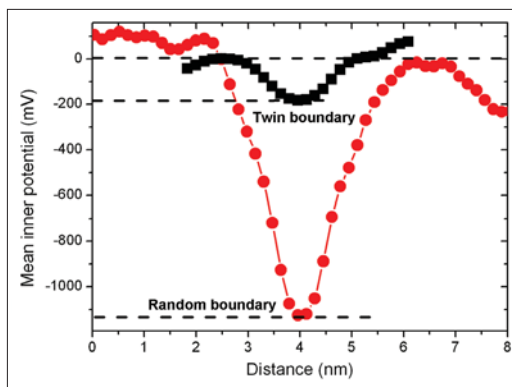


Fig. 3: Mean-inner potential profiles across $\Sigma 3$ (twin) boundaries (black) and random boundaries (red), obtained from phase images, which were reconstructed by the evaluation of Fresnel fringes in transmission electron microscopy focus series.

plained by a variation in the electrostatic potential around the grain boundary. The estimate of free charge carriers includes the free carriers generated by the electron beam in the experiment and was calculated to be lower than $2 \times 10^{15} \text{ cm}^{-3}$. This suggests that the MIP well detected at the grain boundary is likely to be due to a change in composition at the grain boundary.

EBSD and CL images were acquired from solar cells using the related chalcopyrite absorber material CuInS_2 (not shown here). These measurements provide direct access to local crystal orientations, grain boundary types and recombination properties. Across several grain boundaries in the CuInS_2 absorber layer, CL linescans were extracted with the detection wavelength centred on the band-

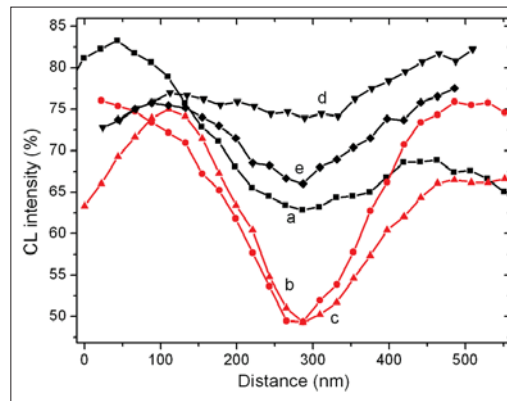


Fig. 4: Profiles extracted from CL images across $\Sigma 3$ (twin) boundaries (black) and random boundaries (red).

band transition, which is dominant at room temperature. As shown in Figure 4, the CL signal is much reduced at random boundaries (Figure 4, curves b and c) and may be explained by a higher density of defects, acting as (non-radiative) recombination centres. In contrast, this density appears to be significantly smaller at $\Sigma 3$ (twin) boundaries. In conclusion, the results suggest that $\Sigma 3$ (twin) boundaries in chalcopyrite-type thin films are electronically less active than random boundaries, as has already been revealed for adamantite systems [3]. A certain density of recombination centres can be expected for all grain boundary types in $\text{Cu}(\text{In,Ga})\text{Se}_2$ or CuInS_2 . However, the recombination velocities revealed are rather low, which gives rise to the assumption that there is a mechanism, e.g. a change in composition, which results in a partial compensation of electrically active defects at grain boundaries. In-line electron holography measurements also show a possible compositional difference between grain boundaries and grain interiors.

The authors are grateful to N. Blau, C. Kelch, M. Kirsch, P. Körber and T. Münchenberg for solar-cell processing, and to U. Bloeck and P. Schubert-Bischoff for help in sample preparation.

- [1] D. Abou-Ras, C.T. Koch, V. Küstner, P.A. van Aken, U. Jahn, M.A. Contreras, R. Caballero, C.A. Kaufmann, R. Scheer, T. Unold, H.-W. Schock, to be published in *Thin Solid Films* (2009).
- [2] M. Nichterwitz, D. Abou-Ras, K. Sakurai, J. Bundesmann, T. Unold, R. Scheer, H.W. Schock, to be published in *Thin Solid Films* (2009).
- [3] E. Billig, M.S. Ridout, *Nature* 173 (1954) 496.

Corresponding author:

Daniel Abou-Ras
daniel.abou-ras@helmholtz-berlin.de

Insights into structure and microstructure of thin films by grazing incidence X-ray diffraction

S. Schorr, Ch. Stephan, H.-W. Schock

■ Helmholtz-Zentrum Berlin für Materialien und Energie, Berlin, Germany

Surface sensitive X-ray diffraction can be achieved by using small incidence angles and a multilayer mirror to produce a parallel incoming beam. Because wave penetration is limited, grazing incidence X-ray diffraction (GIXRD) is a powerful method for depth-resolved studies of the structure and microstructure of thin polycrystalline films. The difference to conventional powder X-ray diffraction, which applies the Bragg-Brentano geometry, is that in GIXRD a non-symmetric configuration of incident and reflected beam is used (Figure 1). Thus the lattice plane which fulfils Bragg's law and contributes to a Bragg peak is not parallel to the sample surface. The incident angle is very small (usually between 0.5° and 5°). A GIXRD experiment consists of several detector scans (2θ -scan) measured with different incident angles (0.5° - 5.0°). By increasing the incident angle, the X-ray penetration depth increases, thus revealing structural information from different depths within the thin film.

GIXRD is the method of choice for studying the structure and microstructure of absorber and buffer layers in thin film solar cells. The benefits are that it is non-destructive and fast; moreover, no sample preparation is necessary.

A few characteristic examples will be presented here. Two of them deal with the structure and

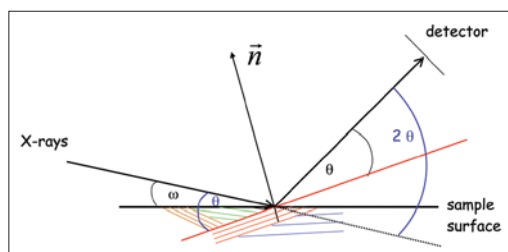


Fig 1: Principle geometry of a GIXRD experiment. The angles are named as follows: ω – incident angle, θ – Bragg angle. The lattice plane normal is marked by \vec{n} .

phase content of polycrystalline thin films within a thin film solar cell. The $\text{Cu}(\text{In,Ga})\text{Se}_2$ (CIGSe) absorber is characterised by variations in the Ga content from the top to the bottom of the layer, resulting in a variation in the structural and electronic properties. To investigate this Ga gradient, GIXRD is applied. Analysing the shift in the Bragg peaks of the chalcopyrite type phase, the Ga content can be determined according to depth. Analysing the intensity ratios between the main Bragg reflections, information about the preferred orientation of the layer can be obtained. It should be noted that the Ga gradient determined by GIXRD closely corresponds to values resulting from an EDX (energy dispersive X-ray) analysis of the absorber profiles. To create the p-n junction of the thin film solar cell, a buffer layer is deposited on top of the absorber layer. This more complex layer structure will be discussed in the third example.

(1) Low temperature growth of $\text{Cu}(\text{In,Ga})\text{Se}_2$ thin film solar cells on polyimide substrates

Lightweight, flexible $\text{Cu}(\text{In}_{1-x}\text{Ga}_x)\text{Se}_2$ (CIGSe) thin film solar cell modules, which are very attractive for space applications, can be produced by the deposition of the CIGSe absorber on a flexible substrate, e.g. polyimide foil (PI).

The structure of a CIGSe absorber layer on PI was studied by GIXRD [1]. The diffraction pattern taken at different incident angles (0.5° - 5°) revealed the presence of several CIGSe phases with chalcopyrite type structure but different Ga content (Figure 2). Analysing the shift in the 112 Bragg peak of the different phases, the Ga content was determined. The changes in the measured peak profile de-

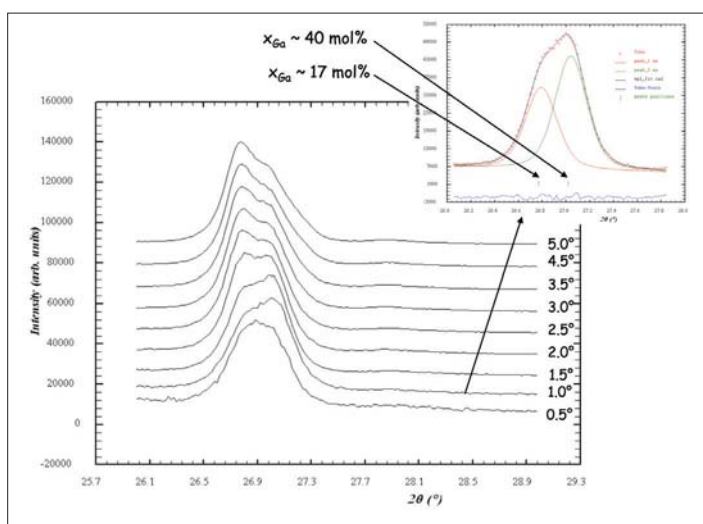


Fig. 2: Part of the GIXRD diffraction pattern (112 Bragg peak) of a $\text{Cu}(\text{In}_{1-x}\text{Ga}_x)\text{Se}_2$ polycrystalline thin film with chalcopyrite type structure deposited on PI. The inset shows the multi-peak fit, corresponding to two phases with different Ga content.

pending on the incident angle indicated a strong Ga content within the layer. Detailed analyses have revealed that the absorber surface is Ga rich ($x_{\text{Ga}} \sim 40\%$) and the Ga content decreases to $x_{\text{Ga}} \sim 17\%$ on the Mo back contact within the layer.

(2) Structural investigations of the first stage of the $\text{Cu}(\text{In,Ga})\text{Se}_2$ three-stage process

A well established method, the three-stage co-evaporation process, was used for growing polycrystalline $\text{Cu}(\text{In,Ga})\text{Se}_2$ (CIGSe) thin films, used as absorber layers in thin film solar cells. In the first stage, In, Ga and Se were deposited as a Ga-Se/In-Se/Ga-Se/InSe sequence to form the precursor layer. The structure and microstructure of the subsequent phases, which depend on the substrate temperature, were studied by GIXRD [2]. The diffraction pattern showed the existence of $(\text{Ga}_x\text{In}_{1-x})_2\text{Se}_3$ mixed crystals with varying Ga content. By increasing the substrate temperature the intermixing of In and Ga was also increased (see Figure 3). In addition to the Bragg peaks of $\gamma\text{-In}_2\text{Se}_3$, it was possible to identify $(\text{Ga}_x\text{In}_{1-x})_2\text{Se}_3$. Moreover, changes in the microstructure were revealed depending on the substrate temperature: At a low substrate temperature the $\gamma\text{-In}_2\text{Se}_3$ layer was microcrystalline; with increasing temperature the size of the crystallites increased. Thus it became obvious that in a standard three-stage process the deposition sequence Ga-Se/In-Se/Ga-Se/InSe in the first stage does not result in a stack of $\gamma\text{-In}_2\text{Se}_3$ and Ga_2Se_3 . The precursor is formed by $(\text{Ga}_x\text{In}_{1-x})_2\text{Se}_3$ mixed crystals with varying Ga content resulting in a thin film with a slight Ga gradient.

(3) Structure of sputtered In_xS_y buffer layers in $\text{Cu}(\text{In,Ga})\text{Se}_2$ thin-film solar cells

In_xS_y layers – used as a buffer in CIGSe thin-film solar cells – were deposited by magnetron sputtering on CIGSe/Mo/glass stacks at three differ-

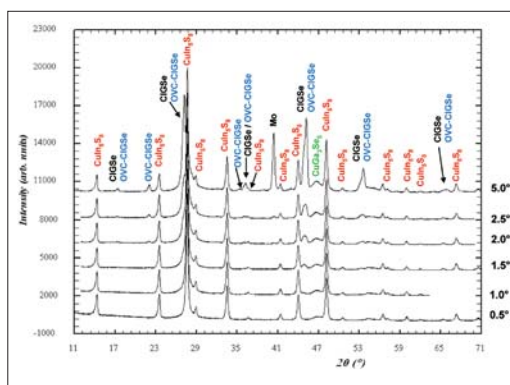


Fig. 4: GIXRD pattern of the 340 °C sample, measured at various incident angles (values given on the right). Peaks attributed to various phases are indicated.

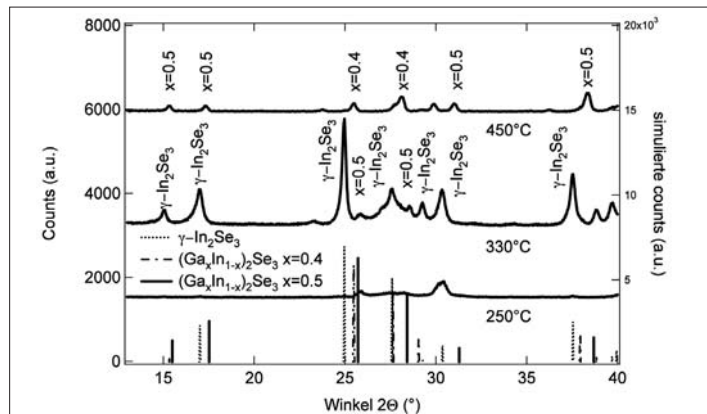


Fig. 3: GIXRD-measurements (incident angle 2°) of In-Se/Ga-Se layers deposited at various substrate temperatures. The Bragg peaks of $\gamma\text{-In}_2\text{Se}_3$ and $(\text{Ga}_x\text{In}_{1-x})_2\text{Se}_3$ ($x=0.4$ and 0.5) are indicated.

ent temperatures (without any heating, at 230°C and at 340°C) and studied by means of GIXRD [2]. The GIXRD diffraction pattern showed that with increasing deposition temperature, new phases were formed by the diffusion of Cu and Ga from CIGSe into In_xS_y and the diffusion of In from In_xS_y into CIGSe. These phases, identified by their Bragg peaks, are the spinel-type phase CuIn_5S_8 and the ordered vacancy compounds (OVC) $\text{Cu}(\text{In}_{1-x}\text{Ga}_x)_5\text{Se}_8$ and CuGa_3Se_5 . The latter exhibits a microcrystalline structure which causes a broadening of the corresponding Bragg peaks. GIXRD measurements taken at different incident angles ($0.5^\circ\text{-}5^\circ$) revealed the stacking of the different phases according to $\text{CuIn}_5\text{S}_8 / \text{CuGa}_3\text{Se}_5 / \text{Cu}(\text{In}_{1-x}\text{Ga}_x)_5\text{Se}_8 / \text{Cu}(\text{In,Ga})\text{Se}_2 / \text{Mo}$ (Figure 4). Moreover, by evaluating the 112 Bragg peak position and applying Vegard's rule, the Ga content of the $\text{Cu}(\text{In}_{1-x}\text{Ga}_x)_5\text{Se}_8$ phase and the $\text{Cu}(\text{In}_{1-x}\text{Ga}_x)_5\text{Se}_8$ phase was determined to be $x \sim 31\%$ and $x \sim 28\%$, respectively.

These are just a few examples of a number of different applications of the GIXRD technique which demonstrate the variety of information on phase content, structure, microstructure and even chemical composition which can be gained by careful analysis of GIXRD data.

- [1] Ch. Kaufmann, R. Caballero, T. Unold, R. Hesse, S. Schorr, M. Nichterwitz, H.-W. Schock, *Sol. En. Mat. Sol. Cells* (2008) in press
- [2] R. Hesse, R. Caballero, D. Abou-Ras, T. Unold, C. A. Kaufmann, H.-W. Schock, *SPIE Optics+Photonics*, San Diego (2007)
- [3] D. Abou-Ras, G. Kostorz, D. Hariskos, R. Menner, M. Powalla, S. Schorr, and A.N. Tiwari, *Thin Solid Films* 517 (8) (2009) 2792-2798.

Corresponding author:

Susan Schorr
susan.schorr@helmholtz-berlin.de

We have take off: $\text{Cu}(\text{In,Ga})\text{Se}_2$ thin film solar cells – recent developments in space applications

C.A. Kaufmann, R. Caballero, R. Scheer, P. Körber, H.-W. Schock (HZB-SE3), R. Klenk (HZB-SE2)
 G. Oomen, C. Hofkamp (Dutch Space B.V., P.O.Box 32070, 2303 DB Leiden, the Netherlands)
 ■ Helmholtz-Zentrum Berlin für Materialien und Energie, Berlin, Germany

Over the last few years, flexible $\text{Cu}(\text{In,Ga})\text{Se}_2$ (CIGSe) thin film technologies have attracted increasing interest due to their potential for space applications. What is behind it? The answer is

- high power-to-weight ratio, i.e. the technology is very light,
- high packing density,
- tolerance of space radiation that is superior to that of crystalline space technologies for photovoltaic power generation [1]
- and low cost.

The Helmholtz-Zentrum Berlin, formerly Hahn-Meitner-Institut Berlin, has been working on the development of flexible CIGSe thin film solar cells on titanium foil substrates for space and terrestrial applications [2,3] since 2002. This work has largely been funded by ESA and undertaken in collaboration with the Zentrum für Sonnenenergie- und Wasserstoff-Forschung Baden-Württemberg (ZSW) in Stuttgart, and Dutch Space B.V. in the Netherlands. A single solar cell device (27.1 cm², AM1.5, without anti-reflective coating) with conversion efficiency of 15% [2] and a mini-module (4 cells, aperture area 108.4 cm², AM1.5, without anti-reflective coating) with aperture efficiency of 12.6% [3] have been demonstrated, in both cases on titanium foil substrates. On a smaller scale, we have made devices in our labs with conversion efficiency of 17% (0.5cm², AM1.5, without anti-reflective coating).

After laborious testing of the CIGSe thin film devices in phase 3 of the ESA TFSC programme, the solar cells were finally deemed fit to be included on a test flight of the Delfi-C3 mission at an orbit of 630 km [4]. This mission was extremely important not only as a test for CIGSe thin film technology on titanium foil itself, but also for the interconnection technology and a high-ε coating that were both specifically developed for devices on flexible conductive substrates by Dutch Space. Figure 1 shows a blow-up schematic diagram of the mini-module assembly, of which 4 have been integrated into the Delfi-C3 micro satellite. Launched on

28 April 2008, the mission has been a complete success so far and the solar cells are in perfect working order at the time of writing this article (Nov 08). About 150,000 sets of I-V curves have been recorded, one of which is shown in Figure 2. Although it would be critical for further evaluation to ascertain the in-flight AMO efficiency of the mini-modules in space, this is difficult to do: Delfi-C3 is a tumbling satellite and it is not easy to determine whether the solar cell surfaces are oriented towards the sun. Furthermore, it is also necessary to take account of albedo-earth shine, the brightness of the earth.

Recent developments in the area of epitaxially grown triple junction (3J) solar cells, based on III-V compounds, have shown the feasibility of greatly reducing the thickness of single 3J devices while maintaining an efficiency level approaching 30%. Although these thin single cells are flexible in principle, they still need support structures to ensure the system's stability during launching and protection against radiation. Despite this, ESA considers this development so promising that it has called a halt to further funding of CIGSe based technology development [5]. However, CIGSe technology, as flown on Delfi-C3, will have another chance to be tested in space when it is incorporated in the MISSE7 mission. It will fly on board the ISS for a year, starting in 2009. This has the advantage that after the flight the assembly will be returned to earth and can be analysed with a view to further optimisation.

Meanwhile, HZB has been working on the transfer of CIGSe technology to a polyimide (PI) substrate. This work is funded by Deutsche Luft- und Raumfahrt (DLR) and is being conducted together with the scientific partner, ZSW, and the industrial partners, Solarion AG, Leipzig and HTS GmbH, Dresden. CIGSe solar cells consist of a layer stack in the order Mo/CIGSe/CdS/i-ZnO/ZnO:Al. Molybdenum is the back contact material. CdS, deposited by chemical bath deposition, is used as a buffer layer between the p-type semiconductor CIGSe absorber layer and the n-type semiconductor i-ZnO/ZnO:Al transparent front contact. The devices are generally completed with a Ni/Al front contact grid which is deposited onto the ZnO front contact in



Fig. 1: Blow-up schematic diagram of the CIGSe thin film solar cell mini-module assembly as flown on Delfi-C3 (the temperature strip determines the temperature of the device).

order to facilitate current collection. Prior to CIGSe deposition a NaF precursor layer is evaporated onto the Mo back contact. The challenge posed by using PI as substrate foil is the large thermal expansion coefficient of the material and in particular its low stability at temperatures above 420°C. On titanium and glass substrates high efficiency CIGSe absorber layers are generally deposited at temperatures above 500°C. In order to optimise the CIGSe growth process for low temperatures, it was found that the amount of Na was critical. At low growth temperatures the sodium influences the layer morphology, the In-Ga interdiffusion during the growth process and the charge density of the resulting CIGSe absorber layer [6]. Figure 3 shows a cross-sectional scanning electron microscope image of just such a CIGSe thin film solar cell on a PI substrate. The whole solar cell is only a few micrometres thick. By optimising both the sodium content and the growth temperature it has been possible to achieve efficiency of, so far, up to 13.6% for the total area on a 0.5 cm² device under AM1.5 illumination and without an anti-reflective (AR) coating (see Table 1). The current record efficiency for low temperature devices on PI foil is 14.1% (total area) which was grown without sodium during CIGSe deposition. Here the Na has been added via a post deposition process [7]. Introducing the sodium after the CIGSe absorber has been finished is known to be beneficial as the layer formation process is not impeded by the presence of Na. The collaborative project on the development of flexible CIGSe technology on PI foils is aiming to produce highly efficient, large area, single solar cell devices of 4×8 cm² in order to demonstrate the future low cost potential of flexible CIGSe solar cell technology - not only for space but also for terrestrial applications.

- [1] A. Messenger, R. Walters, G. Summers, T. Morton, G. La Roche, C. Signorini, O. Anzawa and S. Matsuda, A Displacement Damage Dose Analysis of the Comets and Equator-S Space Solar Cell Flight Experiments, Proc. 16th European PVSEC, 1-5 May 2000, Glasgow, United Kingdom
- [2] A. Neisser, C.A. Kaufmann, R. Klenk, R. Scheer, H.-W. Schock, M.A. Kroon, G. Oomen, D. Herrmann, F. Kessler, M. Powalla, Flexible Solar Cells for Space: A new Development based on Chalcopyrite Thin Films, Proc. 7th ESPC, 9-13 May 2005, Stresa, Italy
- [3] C.A. Kaufmann, A. Neisser, K. Sakurai, P. Körber, H.-W. Schock, R. Klenk, M.C. Lux-Steiner, A flexible, Cu(In,Ga)Se₂ based, thin film solar cell module, in Annual Report 2005 – Selected Results, Hahn-Meitner-Insitut Berlin (HMI-B 608), Berlin, 2006
- [4] <http://www.delfic3.nl>

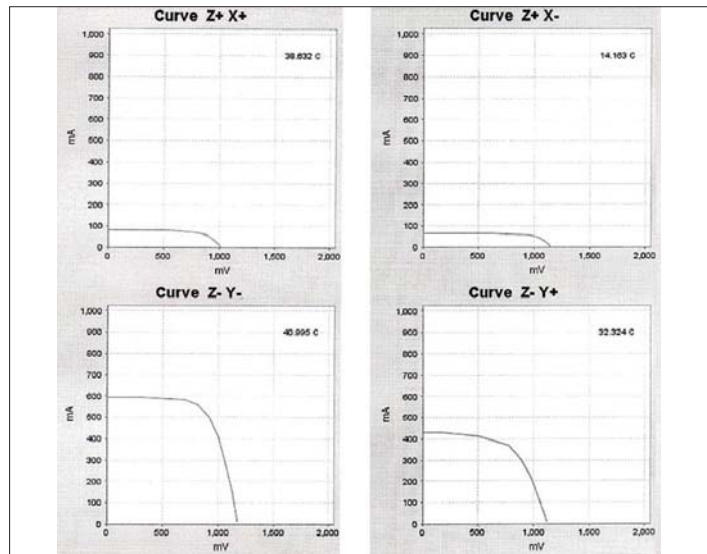


Fig. 2: A full set of I-V curves, of which around 150,000 have been recorded; Z and X indicate the position of the mini-module; the module temperature as indicated by the temperature strip is also given.

- [5] C. Signorini, T. Blancquaert, G. Dudley, L. Gerlach, M. Schautz, E. Simon, F. Tonicello, Power and Energy Conversion Technology: ESA R&D Roadmap and Applications, Proc. 8th ESPC, 14-19 Sep 2008, Constance, Germany
- [6] R. Caballero, C.A. Kaufmann, T. Eisenbarth, T. Unold, S. Schorr, R. Hesse, R. Klenk and H.-W. Schock, The effect of a NaF precursor on low temperature growth of CIGS thin film solar cells on polyimide substrates, Proc. 16th ICTMC, 15-19 Sep 2008, Berlin, Germany - accepted for publication in Physica Status Solidi
- [7] D. Rudmann, D. Brémaud, H. Zogg and A.N. Tiwari, Na incorporation into Cu(In,Ga)Se₂ for high-efficiency flexible solar cells on polymer foils, Journal of Applied Physics 97, 084903

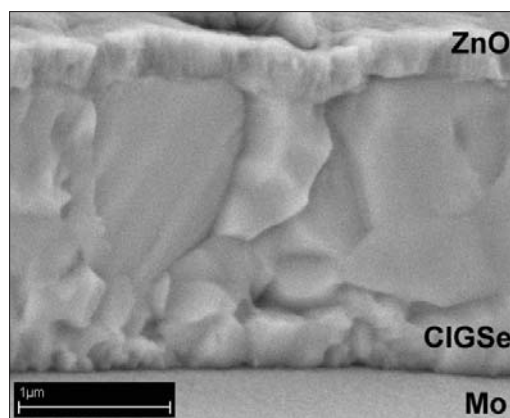


Fig. 3: X-sectional scanning electron microscopy image of the layer structure of a CIGSe thin film solar cell deposited onto PI foil.

Corresponding author:

C.A. Kaufmann
 kaufmann@helmholtz-berlin.de

In-situ control and verification of single-domain III-V growth on Si substrates

H. Döscher¹, T. Hannappel¹, B. Kunert², K. Volz², W. Stolz²

■ 1 Helmholtz-Zentrum Berlin für Materialien und Energie, Berlin, Germany

■ 2 Philipps-Universität, Marburg, Germany

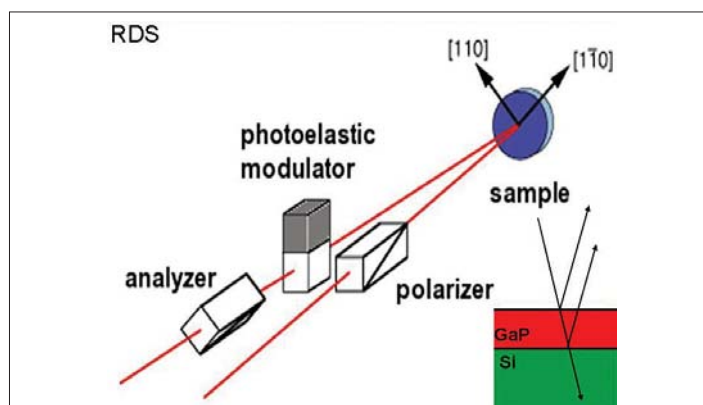


Fig. 1: Measurement principle for RAS. The sample's surface is illuminated in normal incidence geometry with light polarised in two perpendicular directions from the surface. The observed difference in reflection is extremely surface sensitive for all materials with inversion symmetry in the lattice structure.

This work on the in-situ quantification of the surface domain structure of thin gallium phosphide (GaP) films grown on Si(100) [1] was recently awarded, by an independent committee, the 'LayTec In-situ Monitoring Award'. The work was the result of a close collaboration between Helmholtz-Zentrum Berlin für Materialien und Energie and Philipps-Universität, Marburg.

In-situ reflectance anisotropy spectroscopy (RAS, Fig.1) was used for the quantification of antiphase domains on the surfaces of thin GaP films, deposited onto Si(100) by metal-organic vapour phase epitaxy (MOVPE). For the first time, single-domain III-V growth on silicon (100) was determined via the analysis of RAS peak intensities in reference to homoepitaxially grown GaP(100). The in-situ signals were directly correlated (benchmarked) to surface sensitive, UHV-based tools. More specifically, the surfaces were observed with scanning tunnelling microscopy (STM), low energy electron diffraction (LEED) and photoemission (PES). Both pre-processed Si(100) substrates and MOVPE-grown GaP/Si(100) films were also characterised ex-situ, by atomic force microscopy, to identify the formation of mono- and diatomic surface steps and to analyse of the domain distribution, respectively.

The integration of III-V-based opto-electronic devices on to the standard silicon (100) substrates that are used by the established micro-electronic industry is considered to be a major challenge for the semiconductor industry. In photovoltaics, this would allow the combination of high efficiency, multi-junction solar cells with Si(100)-substrates, which would be both competitive and superior in many technological aspects. In addition, there is generally a strong scientific and technological interest in the realisation of III-V semiconductor hetero-epitaxy on silicon substrates, in particular, the industrial scalability of the metal-organic vapour phase epitaxy (MOVPE) technique.

However, the material properties of III-V semiconductors are especially susceptible to lattice defects, and the growth on a non-polar substrate, like silicon, creates additional defect mechanisms [2]. In particular, anti-phase domains (APDs) are typically initiated at the III-V/Si(100) interface during hetero-epitaxial deposition and usually propagate with growth. For the specific study of this crucial defect mechanism, pseudomorphic GaP films were grown on Si(100) by MOVPE and characterised by optical in-situ spectroscopy. Well-ordered GaP/Si(100) surfaces formed by hetero-epitaxial deposition could potentially be used as quasi-substrates, for the integration of III-V-based devices on Si(100) substrates. An in-situ technique for reliably determining the single-domain character of large-area surfaces is essential for the application of GaP/Si(100) quasi-substrates. In normal incidence geometry, RAS shows the normalised difference in the reflection of light, polarised in two perpendicular directions from the surface, $\Delta r/r$ (Figure 1). In materials with inversion symmetry, the bulk does not contribute to the sample's anisotropy and in these cases it causes the desired surface sensitivity of RAS. Different terminations have been identified and were assigned to characteristic RD spectra (Figure 2a) [3]. In the current experiment, the atomic structure of the standard GaP(100) surface was essentially formed by buckled P dimers stabilised by a hydrogen atom (Figure 2b). On the Si(100) surfaces even- and odd-numbered atomic steps can occur resulting either in a (2x1)/(1x2) two-domain surface or a single domain surface reconstruction [4].

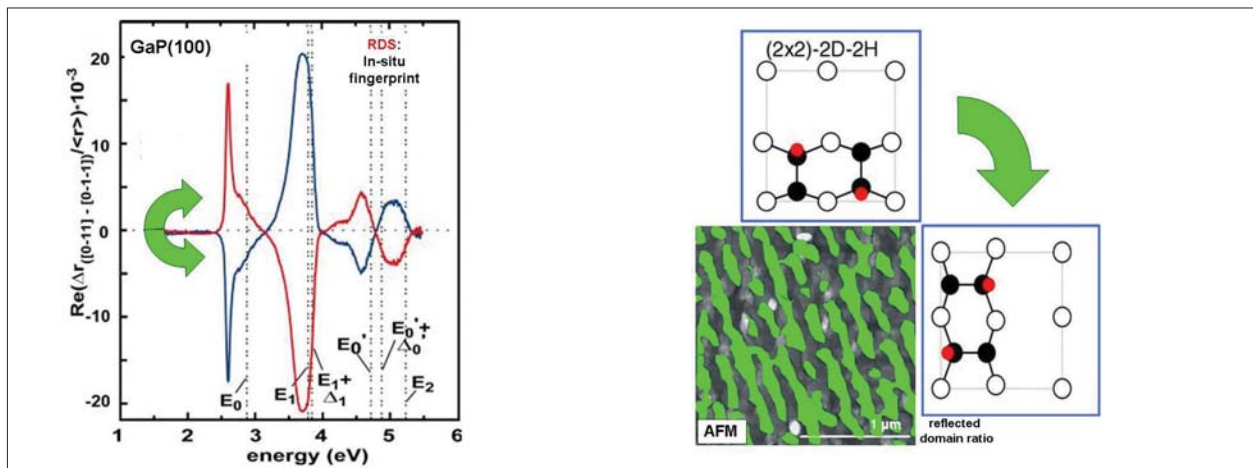


Fig. 2a: In-situ RAS signal of the P-rich GaP(100) surface at 20K. The spectrum shows two extremely intense structures peaking at about 2.6 eV and 3.8 eV, respectively (blue curve). The signal is inverted if the surface directions are exchanged against its definition (red curve).

Fig. 2b: Atomic structure of standard GaP and AFM picture of a hetero-epitaxial GaP film deposited on Si(100). Standard preparation leads to the extensive formation of defective anti-phase domains (coloured in green). In the surface areas, the unit cell of the surface reconstruction is rotated by 90°.

In this experiment, RAS was successfully employed to measure the APD density over the entire spot size (about 0.5 cm²) by correlating the RAS “fingerprints” and the corresponding surface reconstruction domains under MOCVD growth conditions. According to its definition, RAS signals originating from alternating, vertically aligned domains (e.g., APDs) are reversed. Thus, degradation of the RAS signal intensity occurs corresponding to the relative amount of APDs on

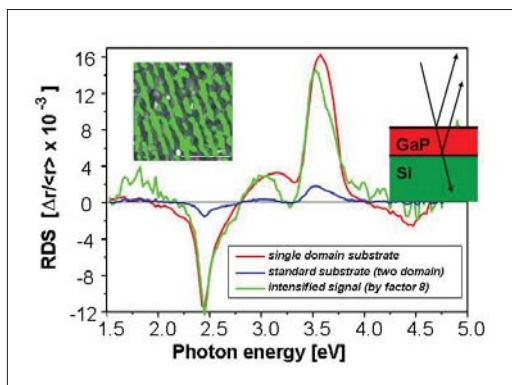


Fig. 3: In-situ RAS/RDS signal for GaP/Si(100) thin films. After an advanced preparation procedure the surface is free of defective anti-phase domains (APDs) as proven by the intense signal (red curve). Samples from standard preparation that contain lots of APDs only give a poor signal (blue curve). Its amplification still reproduces the characteristic RDS peaks and is used for the in-situ quantification of the APD-content.

the surface of the deposited film. In contrast, on Si(100) that is preferentially prepared with biatomic steps, the GaP/ Si(100) surface produces a far less distorted RAS signal with significantly higher amplitude. Hence, the peak intensity at 3.4 eV (Figure 3) correlates directly to the density of APDs. For GaP/Si(100) growth, the maximum RAS amplitude corresponds to a 100% single domain GaP surface with the RAS value of zero indicating a 50:50% distribution for both types of surface domains. These results also provide information about the initial Si(100) surface reconstruction domain ratio prior to GaP epitaxy, as the atomic structure of the Si substrate is a major origin of the detected anti-phase disorder.

In summary, single domain preparation of hetero-epitaxially grown III-V films was demonstrated, in-situ, as being a fundamental contribution to future integration of III-V semiconductors into Si technology. The key issue, that was addressed in this joint result, is the quantitative in-situ measurement of the density of anti-phase domains (APDs) during III-V-epitaxy on Si(100) employing RAS. The analysis of in-situ RAS peak intensities was used for a quantitative measurement of the APD concentration of thin GaP(100) films grown on Si(100) substrates.

- [1] H. Döscher, T. Hannappel et al., Appl. Phys Lett 93 (2008) 172110.
- [2] H. Kroemer, J. Cryst. Growth 81 (1987) 193.
- [3] L. Töben, T. Hannappel et al., Surf. Sci. Lett. 494 (2001) L755.
- [4] D. J. Chadi, Phys. Rev. Lett. 59 (1987) 1691.

Corresponding author:

Thomas Hannappel
hannappel@helmholtz-berlin.de

The Ultrafast Temporal and Spectral Characterisation of Electron Injection in ZnO and TiO₂ based hybrid systems

J. M. Szarko, A. Neubauer, A. Bartelt, L. Socaciu-Siebert, F. Birkner, K. Schwarzburg, T. Hannappel, R. Eichberger

■ Helmholtz-Zentrum Berlin für Materialien und Energie, Berlin, Germany

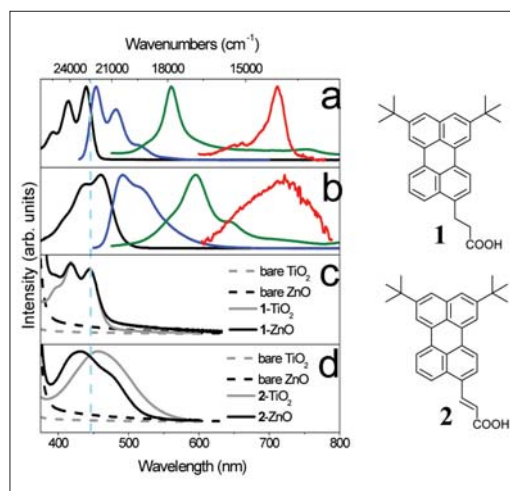


Fig. 1a,b: Absorption and emission spectra of molecules 1 (a) and 2 (b): ground state absorption in methanol (—), emission spectra in methanol (---), cation absorption spectra prepared in concentrated H₂SO₄ (—), and excited state absorption spectra in methanol (---). (c, d) Ground state absorption spectra of molecules 1 (c) and 2 (d) attached to ZnO and TiO₂ colloids. The UV/Vis absorption spectra of the unsensitised colloidal films of ZnO and TiO₂ are also shown. The blue dotted line at 445 nm denotes the central position of the pump beam in the fs Transient Absorption experiment.

ZnO is a promising semiconductor material for charge transport electrodes in low-cost hybrid nano-composite solar cells and may, in the future, eventually replace the widely used colloidal TiO₂ in such devices [1]. ZnO shows enhanced structural and electronic features that could be advantageous for future dye sensitised solar cells (DSSCs). For example, by separating the photo-excited electrons from the cationic dye molecule more quickly, DSSCs made from ZnO nanorods have shown faster electron transport rates which could lead to higher efficiencies. However, TiO₂ DSSCs are currently the most efficient hybrid solar cells with a conversion

efficiency of over 10% [2], whereas ZnO based DSSC efficiencies remain below 6% [3]. Charge separation at the dye/ZnO interface is poorly understood, and reported injection dynamics at ZnO nm-structured electrodes range from hundreds of fs to hundreds of ps and are much slower when compared to TiO₂ [4].

In order to gain a more fundamental insight into the dynamics of the photo-induced electron transfer processes at dye sensitised nanocrystalline ZnO and at TiO₂ electrodes, the two systems were studied and directly compared using Femtosecond Transient Absorption in ultra-high vacuum. Two perylene derivatives were used as model sensitizer chromophores, chemisorbed onto the ZnO and TiO₂ semiconductor surfaces either by a propionic acid (-CH₂-CH₂-COOH) (molecule 1), or an acrylic acid (-CH=CH-COOH) (molecule 2), which respectively discriminated between weak and strong electronic coupling. The molecules differ only in one unsaturated bond that delocalises the excited-state electron over the entire acrylic acid bridge and therefore couples it more closely to the colloidal surface.

The steady state absorption spectra of the ground, cationic and excited states of the perylene derivatives in solution and the ground state absorption of the four dye/semiconductor systems are depicted in Figure 1.

Figure 1c shows the linear ground-state absorption spectra of 1-TiO₂ and 1-ZnO that are similar to the ground state spectra of the molecules in solution. The vibronic peaks are slightly broadened, which is characteristic for electronic coupling and ultrafast electron injection. The ground-state absorption spectra of molecule 2 attached to TiO₂ or ZnO colloids (Figure 1d) do not show the vibronic progression, which indicates an even stronger electronic coupling and faster electron injection. This trend is confirmed by the fs pump-probe measurements exciting the perylene dyes at 440 nm and probing with an ultra-short white-light continuum. The experiment simultaneously monitored the evolution of

the cationic and excited state dynamics in a broad spectral window (Figures 2 and 3).

The transient absorption spectra for the systems 1-ZnO and 2-ZnO are characterised by three main components (Figure 2). The area from 630–750 nm shows an instantaneous rise-time due to the excited-state species that decreases in a time window from 100 fs to 1 ps. The 550–620 nm region shows an increase in time due to the rise of the cationic signal, as the electron is transferred from the molecule to the semiconductor. The measured time constants for the cationic state rises and for the excited state decays at early times (ranging from 200 to 250 fs for the two systems), showing a complimentary behaviour suggestive of direct electron transfer from the excited state of the adsorbed molecule into the semiconductor. This is further supported by an isosbestic point observed at 625 nm, indicating that only two species are present in the depicted time range. The negative signal from 530–550 nm is ascribed to the ground state bleaching of the chromophore quenched by ultrafast electron transfer.

The transient absorption spectra of 1-TiO₂ (Figure 3a) look similar to the 1-ZnO spectra, but the cationic peak for the 1-TiO₂ system is more pronounced due to a larger percentage of the excited-state being already depleted within the duration of the exciting laser pulse, due to faster electron injection. The injection time is much shorter for this system, being 57 fs, as previously reported [5]. The transient absorption spectrum of 2-TiO₂ (Figure 3b) shows a large negative signal at 530–550 nm (ground-state bleaching) which is attributed to an ultrafast direct charge transfer that competes with the excited state at 710 nm. The cationic state rise-time in this system was previously reported as 10 fs [5].

In conclusion, the injection dynamics of the ZnO based systems was found to be slower compared to the TiO₂ counterparts but show a similar trend in dynamics making it a good candidate for DSSCs. The injection times of around 200 fs for the ZnO based systems are, overall, the shortest for any dye-sensitised ZnO colloid system accurately time-resolved so far.

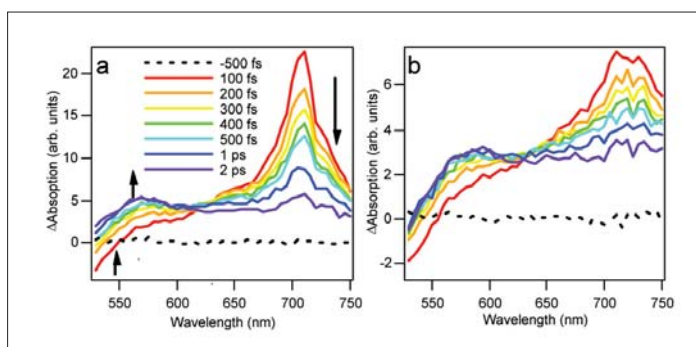


Fig. 2: Transient absorption spectra of 1-ZnO (a) and 2-ZnO (b) showing cationic and excited state dynamics

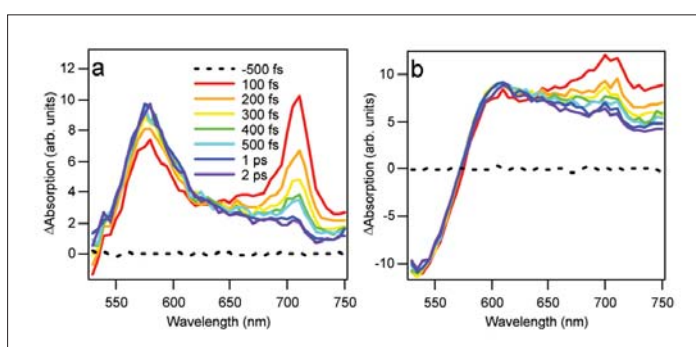


Fig. 3: Transient absorption spectra of 1-TiO₂ (a) and 2-TiO₂ (b) showing cationic and excited state dynamics.

- [1] M. Law, L. E. Greene, J. C. Johnson, R. Saykally, P. Yang, *Nat. Mater.* 4, 455 (2005)
- [2] M. Grätzel, *Nature* 414, 338 (2001)
- [3] K. Keis, E. Magnusson, H. Lindström, S. Lindquist, A. Hagfeldt, *Sol. Energ. Mat. Sol. C.* 73, 51 (2002)
- [4] J. M. Szarko, A. Neubauer, A. Bartelt, L. Socaciu-Siebert, F. Birkner, K. Schwarzburg, T. Hannappel, R. Eichberger *J. Phys. Chem. C* 112, 10542 (2008)
- [5] Ernstorfer, R., Ph.D. Thesis, Freie Universität Berlin, 2004

Corresponding author:

R. Eichberger
eichberger@helmholtz-berlin.de

Development of a membrane for photo-induced hydrogen generation

S. Fiechter, H.J. Lewerenz, P. Bogdanoff

■ Helmholtz-Zentrum Berlin für Materialien und Energie, Berlin, Germany

It is well known that solar cells are able to convert sunlight into electrical energy. As sunlight is not permanently available, however, a part of this energy has to be stored, for example, by using rechargeable lithium batteries. Another option is the storage of chemical energy in the form of hydrogen, produced by water splitting via solar energy. Compared with battery systems and hydrocarbons such as benzene or diesel, hydrogen has an extraordinarily high energy density and can be stored in pressurised bottles or as metal hydrides. The low weight of hydrogen and its high energy content also make it attractive as fuel for mobile applications. By comparison: 6kg H₂ correspond to 200kWh of chemical energy while the weight of a 540kg lithium ion battery is needed to deliver 100kWh of electrical energy. Subsequent conversion of this chemical energy into electricity by a fuel cell system (typical efficiency: 50%) means that the overall energy conversion efficiencies are comparable. Since cheap metal hydrides are not yet available for technical application, compressed hydrogen has to be stored in dedicated containers. Based on present technology, the system weight of 125kg (H₂) still compares favourably with a battery system weighing 830kg.

Thus to store chemical energy in the form of hydrogen efficiently, novel storage systems (e.g. metal hydrides, methanol) as well as efficient energy

converting systems have to be developed in order to use sunlight as a virtually inexhaustible, renewable energy source. Therefore to envisage a future hydrogen economy, efficient catalysts and efficient energy converting devices have to be developed. In contrast to the process of photosynthesis in which non-noble metal catalysts (Mn- and Fe-Ni-clusters) convert CO₂ and water into O₂ and hydrocarbons, current artificial systems - combining solar cells with an electrolyser - employ platinum and ruthenium oxide in the process of water splitting. One of the intriguing research goals is therefore the mimicking of the thylakoid membrane in plants. Thus the development of an artificial "water splitting membrane", allowing the direct conversion of sunlight into hydrogen and oxygen, is of particularly high importance. Approaches that include organic and inorganic systems to achieve this goal have been proposed. The basic problems relate to the stability of organic artificial systems and so we have introduced a design that uses hitherto inorganic components: a thin film photovoltaic monolithic, so called back-to-back tandem structure with integrated catalysts at the photocathode (hydrogen generation) and the photoanode side (oxygen generation) to facilitate water splitting by sunlight (Figure 1).

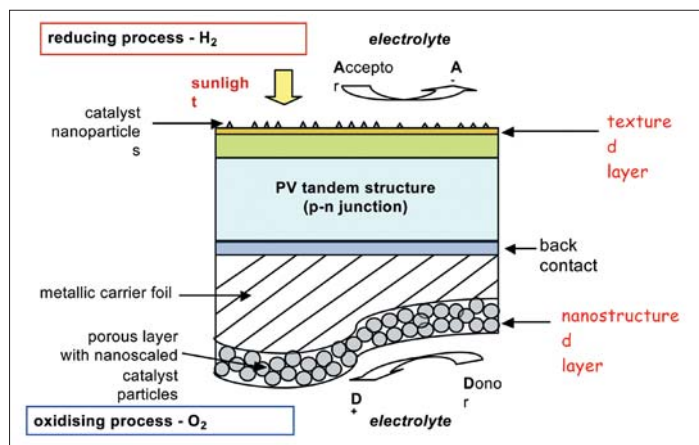


Fig. 1: Schematic cross section of a water splitting membrane combining a thin film tandem solar cell structure with nano-scaled catalysts to generate hydrogen at the cathode and oxygen at the anode side under irradiation of the device with sunlight after immersion in water (adapted from [2]).

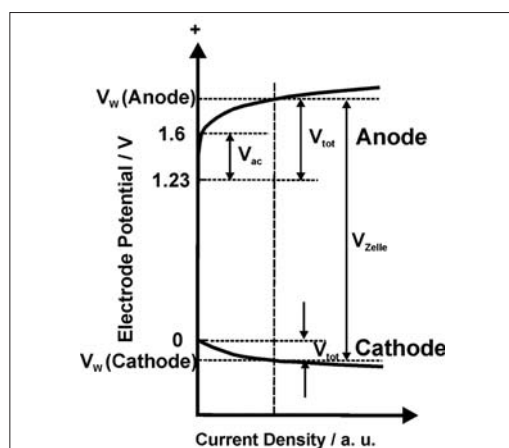


Fig. 2: Schematic representation of the dependency of the current density from the applied potentials V_w on the cathode and the anode sides. The I-U curves shown increase exponentially with increasing current density. The current density particularly increases on the anode side where oxygen evolution occurs during water splitting.

The concept of an integrated monolithic photoelectrochemical-photovoltaic design, splitting water directly upon illumination, was realized for the first time in 1998 by Khaselev and Turner using a high efficiency GaAs-GaInP₂-based tandem structure [1]. At the Helmholtz-Zentrum für Materialien und Energie a first prototype has been constructed by Neumann et al. [2-3] using a chalcopyrite thin film solar cell absorber with a niobium-doped TiO₂ emitter layer and adsorbed platinum particles at the cathode. At the photoanode, a porous TiO₂ layer was used. The photovoltage achieved by the illuminated chalcopyrite solar cell was too small to split water directly because of the small solar photon flux in the spectral region where TiO₂ is absorbed. In order to test the concept further, more intense UV radiation was applied to the anode side to precipitate the process, which did result in water splitting. The main reasons for promoting the general concept of monolithically integrated systems rather than a separate photovoltaic-electrolyser approach are that it seems to promise more technological applications and lower costs [4-5].

The thermodynamic potential of water dissociation reaction according to the chemical equation



is given by the electromotoric force $V_0 = -\frac{\Delta G^0}{nF}$,

where the free Gibb's enthalpy ΔG^0 is defined by $\Delta G^0 = \Delta H^0 - T\Delta S^0$. At pH = 0 and T = 25°C a value of $V_0 = 1.23\text{V}$ is obtained. The main challenges besides the surface stability of the light absorbing material and the stability of the nano-scaled catalysts are posed by so-called overvoltages. In particular, the overvoltage on the anode side, where four electrons have to be transferred via the electrode-electrolyte interface to oxidise two water molecules in order to obtain one O₂ molecule, tends to be high, reaching values of between 0.4 and 0.6V. The size of this value strongly depends on the properties of the catalyst used. Because these overvoltages are an inherent limiting parameter of the process, they affect the efficiency $\eta_{\text{photoelectrolysis}} = \eta_{\text{PV}} \times \eta_{\text{electrolysis}}$ with

$$\eta = \frac{1.23\text{V}}{V_{\text{cell}}}$$

of the process substantially.

Figure 2 shows a schematic energy diagram illustrating the dependency of the working potentials VW at the electrodes of half cells from the current density. Although no numbers are given in the diagram a current density of e.g. 10mAcm⁻² can necessitate a potential V_{cell} which is 30% to 50% higher than the thermodynamic value of 1.23V. Application of these considerations to the semiconductor-electrolyte phase boundary demands that the absolute positions of the semiconductor

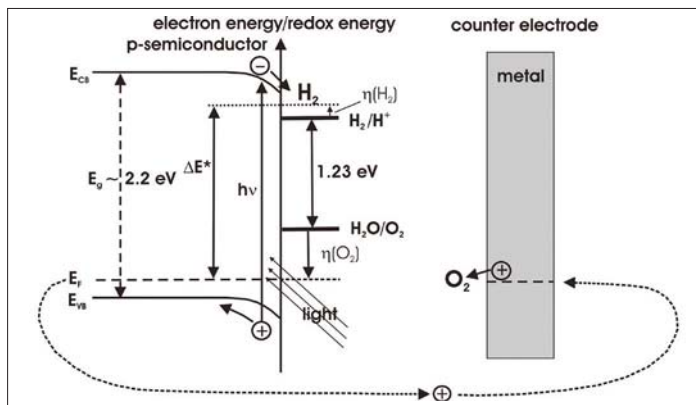


Fig. 2: Overall energetic restraints for the evolution of H₂ and O₂ at semiconductor-electrolyte interfaces; η denotes the overpotentials (VW) in electrochemical notation, ΔE^* is the cell voltage V_{cell} of Figure 2. The system drawn uses a *p*-type semiconductor at which H₂ evolution takes place by electron injection into the electrolyte from the conduction band. O₂ evolution energies are included to visualise the overall energetic situation.

conduction and valence bands are located so that the reduction reaction of protons to H₂ can proceed from the conduction band and the valence band is energetically located below the potential for anodic water decomposition. In addition, with semiconductors, a driving force for charge separation as reflected in the energy band bending is required and resistive losses in the electrolyte and series resistance also have to be taken into account. This adds a value up to about 2.2eV - 2.3eV for the energy gap of a suitable semiconductor. The respective energy diagram is shown in Figure 3 together with the basic fuel generation reaction schemes. With a limiting energy gap of ~2.3eV, the theoretical solar energy conversion efficiency for a single junction is in the range of 14% under AM 1.5 conditions, making tandem structures that evolve hydrogen and O₂ more promising with respect to higher system efficiencies [6].

- [1] O. Khaselev, J. A. Turner; Science 280 (1998) 425.
- [2] H. Tributsch, B. Neumann; International Journal of Hydrogen Energy 32 (2007) 2679.
- [3] B. Neumann, F. Birau, B. Johnson, C. A. Kaufmann, K. Ellmer, H. Tributsch; phys. stat. sol. B 245 (2008) 1849.
- [4] N.S. Lewis, Nature 414 (2001) 589.
- [5] A.J. Bard, M.A. Fox, Acc. Chem. Res. 28 (1995) 141.
- [6] C.A. Grimes, O.K. Varghese, S. Ranjan; Light, Water, Hydrogen, The Solar Generation of Hydrogen by Water Photoelectrolysis, Springer, Berlin, 2007.

Corresponding author:

S. Fiechter
fiechter@helmholtz-berlin.de

Preparation of photoactive WS₂ nanosheets by rapid crystallisation of amorphous WS_{3+x} films: an in situ, real-time X-ray diffraction study

Stephan Brunken¹, Rainald Mientus², Klaus Ellmer¹

■ 1 Helmholtz-Zentrum Berlin für Materialien und Energie, Berlin, Germany

■ 2 Opto-Transmitter-Umweltschutz-Technologie e.V., Berlin, Germany

Tungsten disulphide (WS₂) belongs to the class of layer-type transition metal dichalcogenides (MoS₂, WSe₂, MoSe₂ etc.), which have been investigated for more than 30 years as prospective absorber materials for solar cells [1]. WS₂ crystallises in a hexagonal structure and consists of S-W-S triple layers, which are stacked over each other along the c direction (Fig. 1). Whilst the bonding within the layers is covalent, the bonding between the S-W-S sandwiches (i.e. between sulphur atom planes) is of the van der Waals type (~0.15 eV/S atom). The sulphur-terminated (001) planes are nearly free of dangling bonds, allowing the preparation of good heterojunctions for solar cells of a high electronic quality. The band gap of about 1.8 eV and its very high absorption coefficient (> 10⁵ cm⁻¹) makes WS₂ a candidate as absorber layer in thin film solar cells.

In this research project, the growth of WS₂ layers in the desired (001) orientation was investigated by in-situ, time-resolved energy-dispersive X-ray diffraction (EDXRD) at the synchrotron radiation source HASYLAB in Hamburg. Here a white X-ray beam (6-60 keV) is diffracted at the sample and detected by a germanium detector. The diffraction patterns were measured at a fixed diffraction angle of about 4° with time resolutions of 1-10 seconds during the

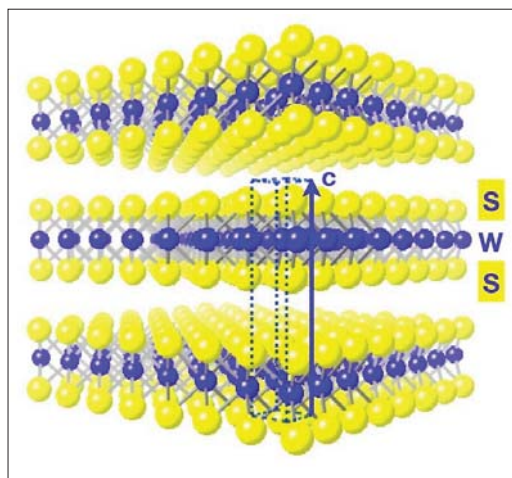


Fig. 1: Crystal structure of WS₂

growth and the crystallisation of the WS₂ films [2, 3]. In order to prepare highly (001)-textured WS₂ films, a procedure first described by the Tenne group [4] was used:

1. Deposition of a thin metal film on the substrate, for instance a nickel film of 5 to 50 nm thickness
2. Deposition of an amorphous film by reactive magnetron sputtering from a tungsten target in an Ar/H₂S gas atmosphere at temperatures <100 °C.
3. Rapid crystallisation of the amorphous WS_{4.5} films to WS₂ by annealing in H₂S atmosphere of about 10 Pa.

The steps 2 and 3 were observed by time-resolved EDXRD and an example is shown in Figure 2, where the Ge-detector count rate (colour coded) is displayed as a function of the photon energy over the annealing time. Initially, only fluorescence peaks of nickel (K_α) and tungsten (L_{α,β}) and a weak diffraction peak (111) of the nickel layer can be seen. The Ni(111) peak vanishes immediately

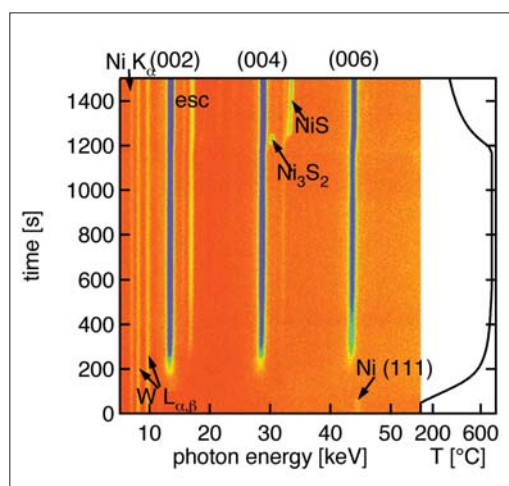


Fig. 2: In-situ real-time EDXRD during an annealing process in H₂S of an amorphous WS_{3+x} film on a nickel-coated oxidized silicon substrate. The intensity of the diffracted synchrotron light is plotted color-coded.

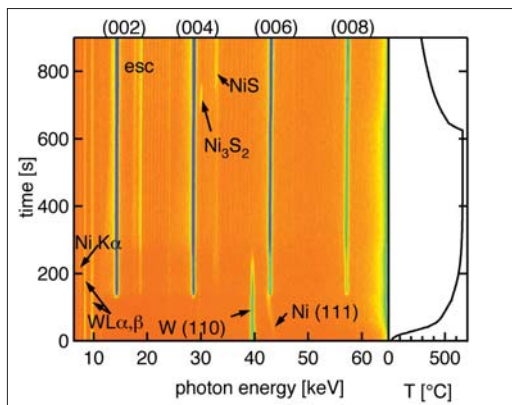


Fig. 3: In-situ real-time EDXRD of an annealing process in H_2S atmosphere of an W film on a nickel-coated oxidized silicon substrate. The intensity of diffracted synchrotron light is plotted color-coded.

after the start of heating. At this moment, $WS_{4.5}$ loses its excess sulphur and converts to WS_2 , and the WS_2 (002) diffraction peaks then start to grow rapidly. Using Rutherford backscattering, it was verified that the sulphur-rich $WS_{4.5}$ films are transformed to stoichiometric WS_2 crystals by evaporation of the excess sulphur at about 300 °C. During

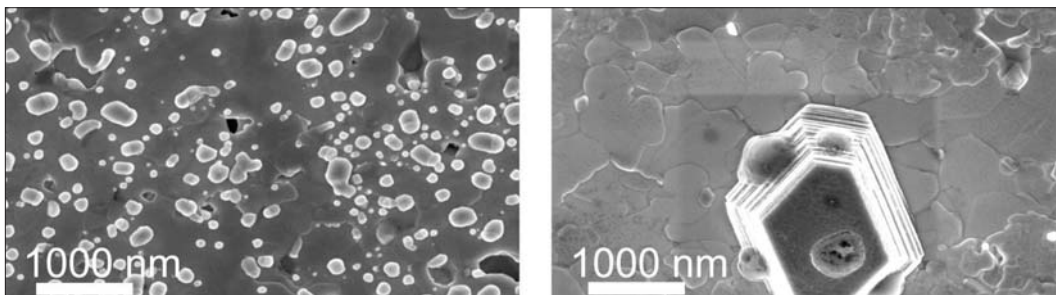


Fig. 4: Scanning electron micrographs of WS_2 films, crystallized on a (a) palladium and a (b) nickel-coated substrate.

cooling the liquid nickel sulphide crystallises and forms the Ni_3S_2 phase and later the more sulphur-rich phase NiS . Nickel also induces the sulphidation of the tungsten film (Fig. 3). With increasing temperature a shift of the nickel (111) peak towards lower energies occurs, which is caused by the dissolution of tungsten in nickel. When Ni (111) disappears, WS_2 (002) grow rapidly and the W (110) diffraction vanishes.

The onset of rapid crystallisation occurs at a temperature of about 650 ± 50 °C. We attribute this crystal growth to the formation of a liquid NiS_x . When oversaturation occurs, highly (001)-textured WS_2 sheets crystallise out of the liquid NiS_x nucleation seeds. As well as nickel, cobalt and palladium can also be used as crystallisation promoters [3].

The morphology of rapidly crystallised WS_2 films using a palladium (a) and a nickel (b) film for crystallisation is shown in Figure 4. The WS_2 crystallites exhibit lateral dimensions of up to 3 μm . Between the large WS_2 nanosheets, smaller NiS_x or PdS_x crystallites can be found, which mostly sit on top of the WS_2 crystallites. When the crystallisation is performed without the promotion of Ni, Co or Pd, the films exhibit very small nanocrystallites, thus proving the essential role of the metal sulphide promoters. From the in-situ, time-resolved EDXRD analysis and from morphological investigations by scanning electron microscopy, a modified model for the rapid crystallisation was established. The crystal growth involves an amorphous solid – liquid – crystalline solid process, which is similar to the well known vapour-liquid-solid process for the growth of nanorods [5].

The rapidly crystallised metal-sulphide assisted WS_2 films exhibit a hole carrier concentration in the range of $10^{17} cm^{-3}$ with a mobility of up to $80 cm^2/Vs$ at room temperature, which is in the same range as the mobility in WS_2 single crystals. These films are photoactive, which was proved by time-resolved microwave conductivity measurements with an excitation wavelength of 532 nm. This suggests that such rapidly crystallised WS_2

nanosheets should be suitable as good absorber layers in thin film solar cells, and this is to be investigated in the near future.

1. Tributsch, H., Ber. Bunsenges. Phys. Chem., 1977. 81: p. 361-369.
2. Brunken, S., R. Mientus, S. Seeger and K. Ellmer, J. Appl. Phys., 2008. 103(6): p. 063501-6.
3. Ellmer, K., Phys. Stat. Sol. (b), 2008. 245(9): p. 1745.
4. Salitra, G., G. Hodes, E. Klein and R. Tenne, Thin Solid Films, 1994. 245(1-2): p. 180-185.
5. Wagner, R.S. and W.C. Ellis, Appl. Phys. Lett., 1964. 4(5): p. 89-90.

Corresponding author:

Stephan Brunken
stephan.brunken@helmholtz-berlin.de